Unified Sample Difficulty Estimation in Pathology Foundation Models

Anonymous authors
Paper under double-blind review

Abstract

The fast scaling speed of histopathology datasets allows researchers to train various foundation models for disease-centered research with applications in classifying disease-state information and predicting gene expression levels. However, it has been shown that current models tend to be overconfident and make classification at a low-calibration level. This case is underexplored for regression-type tasks such as gene expression prediction as well, which could seriously affect the diagnosis and treatment based on the developed models. To resolve this critical issue, we propose a universal framework[1] to estimate the sample difficulty (USD) in both regression and classification tasks. In particular, we fit the data in the embedding space with Gaussian distribution and then utilize prior-informed relative Mahalanobis distance to estimate sample difficulty. Moreover, we incorporate such difficulty as a weight to regularize the model prediction, which can improve model performance by emphasizing challenging samples. Our method can be seamlessly extended to regression tasks by the incorporation of discrete targets. Compared with the second-best method on average, extensive experiments demonstrate that our proposed USD can improve the disease-state classification accuracy by 1.0% at least and gene-level correlation by 3.5% at least using UNI. Finally, we provide comprehensive ablation tests to demonstrate the importance of including sample difficulty in the training stage and case studies for assigning samples with different difficulty levels.

1 Introduction

The analysis of gigapixel-level whole-slide images (WSIs) is an important topic in computational pathology Song et al. (2023a); Bera et al. (2019); Niazi et al. (2019); Al-Janabi et al. (2012). Due to the complexity and scarcity of pathology data, it is difficult for a pathologist to make accurate diagnoses. While machine-learning-based methods have been applied for pathology analysis Neto et al. (2024); Shaban et al. (2024), these models are usually trained with limited data and knowledge, which might not be useful for general purposes Zhang & Metaxas (2024). To solve this issue, extensive efforts have been made to collect large-scale pathology data, bringing in several pathology foundation models (PFM) pre-trained with pathology image or multimodal data Chen et al. (2024b); Lu et al. (2023); Xu et al. (2024a); Ma et al. (2024). Those PFMs generate robust representations for WSIs in either patch level or slide level, which demonstrate state-of-the-art (SOTA) performances for a wide range of tasks including disease-state classification, disease sub-type identification, medical text-image retrieval, etc. Recent research has also explored cases of using features from PFMs to predict gene expressions from hematoxylin and eosin (H&E)–stained images Jia et al. (2024); Xie et al. (2024); Anonymous (2024); Lee et al. (2024b), revealing the potentials in handling regression-oriented problems.

Despite this great progress, we often detect misclassified samples in both training and testing sets when using PFMs for classification-oriented problems. The potential reasons could be multifaceted such as assigning wrong labels, changing brightness, adding medical annotation, etc. Given the importance of diagnostic accuracy for patients Niazi et al. (2019), handling extensive noise in pathology data is highly essential. Although some researchers have investigated the difficulty of training samples in general image datasets (e.g., ImageNet Deng et al. (2009)) with technique development Cui et al. (2023) on relative Mahalanobis

[1]Full codes can be found here: `https://anonymous.4open.science/r/USD-F176/` (also in supplementary files).

distance Mahalanobis (2018) and data distillation Wang et al. (2024), we have not yet found any research that systematically investigates how to process these difficult samples in pathology images. Moreover, most of the current research on sample difficulty focuses on classification-oriented problems and attempts to improve models with enhanced generalization ability Cui et al. (2023), but how to extend the learning of sample difficulty in regression-oriented problems remains unsolved. For spatial transcriptomic data analysis, predicting gene expression information based on the H&E image is also an emerging field, as the measurement of spatial transcriptomics data is expensive Zhu et al. (2025); Zeng et al. (2022) for large-scale analysis. In addition, multi-modal information can provide more insights for pathology analysis Qiao et al. (2022), and thus predicting transcriptomics as a new modality allows us to perform additional analyses such as survival prediction Jaume et al. (2024b) and cell-cell communication inference Armingol et al. (2021). Since we find that these expression predictors might fail for certain genes or spots, we plan to dive deeper for an interpretable solution. Therefore, a general framework for understanding and interpreting sample difficulty for pathology image analysis will be extremely helpful for domain experts in the medical field.

In this paper, we propose a **U**niversal Learning Framework for Estimating **S**ample **D**ifficulty (USD) and improving the capacity of PFMs in histopathology image analysis. Different from previous research Cui et al. (2023); Agarwal et al. (2022); Zhu et al. (2024), our method first transfers the concept of sample difficulty into an outlier detection problem, and then models the training difficulty of samples by integrating the prior information jointly with modified relative Mahalanobis distance (*MRMD*). Furthermore, we leverage discrete targets to extend our sample difficulty to the gene expression prediction task, resulting in a universal model for both regression and classification problems. With these novel designs, USD demonstrates a SOTA performance in both disease-state classification and disease sub-type identification across three datasets of different scales. In addition, USD improves the prediction of gene expression levels from the perspectives of both performance and interpretability across eight datasets from different tissues and diseases.

We further visualize the sample difficulty estimated by USD in Figure 1 and perform clustering analysis in Appendix 6.1. Regarding the disease-state classification task, we can observe an intuitive difference in pathological morphology between the selected samples. We also cannot detect the squamous-like regions enriched with cancer cells in the difficult samples labeled as lung squamous cell carcinoma (LUSC). Regarding the gene expression prediction task, we find that the patches with lower cell enrichment or clear tissue patterns are marked with a high difficulty level, which aligns with their Pearson correlation coefficient (PCC) scores. In contrast, for regions with more useful morphological information, these samples are assigned with lower difficulty, which can be validated by accurate predictions. Overall, our method can help researchers to better select pathological regions and filter out useless information.

Our contributions are: (1) we show that PFMs provide superior slide- and patch-level representations, whose features can also estimate sample difficulty; (2) we introduce *MRMD*, a metric for measuring difficulty in classification and regression with fewer false positives; (3) we demonstrate that combining difficulty-aware learning with entropy regularization improves performance; and (4) we design a difficulty-aware loss that boosts results on over 70% of datasets. Beyond these, we establish novelty by conducting the most comprehensive evaluation of PFMs to date across diverse datasets, tasks, and metrics, proving the generalizability of our solutions beyond UNI and surpassing traditional visual models like ResNet50. We further show, for the first time, that PFM features extend naturally to sample difficulty estimation, adding interpretability to pathology workflows. Finally, ablation and robustness analyses clarify when and why PFMs are essential, linking feature representation with difficulty estimation to advance both regression and classification within a unified framework.

2 Related Work

Pathology Foundation Models (PFMs). Learning robust representations of pathology images is a challenge with extensive applications in computer-aided diagnosis, and PFMs are developed to resolve it. Most of the current PFMs are visual-based or textual-visual-based large-scale neural networks built based on transformer blocks. Moreover, these models diversify in model architectures, pre-training strategy, and training datasets. For example, models such as UNI Chen et al. (2024b) rely on DINOv2 Oquab et al. (2024) as base architecture and Mass-100K dataset in the pre-training stage, while models like GigaPath Xu et al.

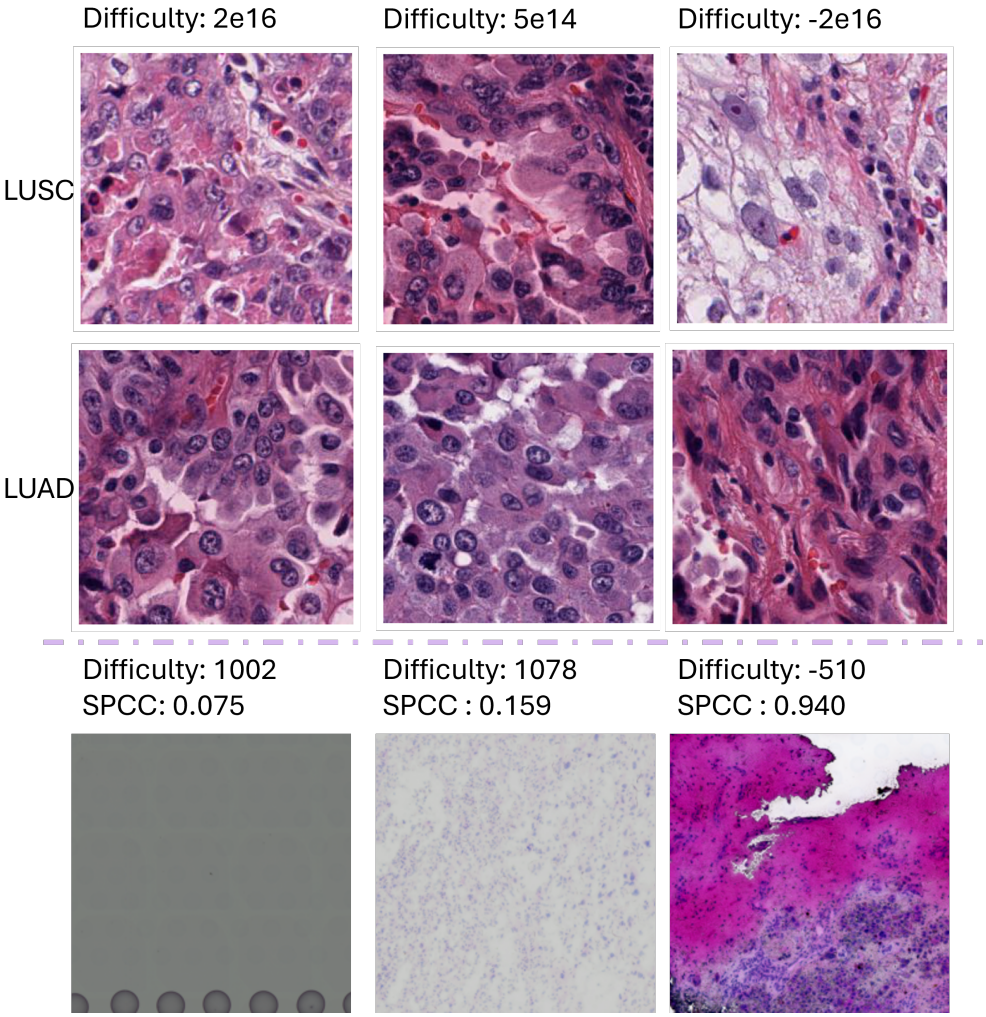

Figure 1: Illustration of sample difficulty (lower means easier) based on histopathology images. The panel above represents the comparison for the classification task based on samples from the TCGA dataset. The panel below represents the comparison for the regression task based on samples from the Brain dataset.

(2024a) is built based on ViT Dosovitskiy et al. (2021) and utilizes private datasets which are not publicly available. Furthermore, models such as PLIP Huang et al. (2023), CONCH Lu et al. (2024), MUSK Xiang et al. (2025), and TITAN Ding et al. (2024) utilize multi-modal information in the pre-training stage, which enlarges the models' capacity in handling the cross-modality tasks. There also exist models focusing on introducing more modalities in the pre-training stage, such as mSTAR Xu et al. (2024b) with transcriptomic data, as explorations for new pre-training frameworks.

PFM Applications. Foundation Models are named after their powerful and wide-ranging downstream capabilities in few-shot and zero-shot learning scenarios, and this is no exception for PFMs. The proposed PFMs have already demonstrated strong abilities in handling disease-related classification tasks, such as disease-state prediction, disease sub-type identification, and image-image retrieval Chen et al. (2024b); Ochi et al. (2024); Xiang & Zhang (2023). These challenges are constrained by data quality and disease heterogeneity and thus they did not have general solutions in the past. Furthermore, PFMs with language capacity can also be applied to addressing multi-modal tasks such as text-image retrieval Huang et al. (2023), visual question answer (VQA) testing Xiang et al. (2025), and medical report generation Shaikovski et al. (2024); Liu et al. (2025b). Recently, researchers also explored the capacity of predicting spot-level gene expression information directly from the paired image information with features obtained from PFMs, which shows potential to help analyze spatial transcriptomics data with lower cost than performing data sequencing directly Anonymous (2024); Lee et al. (2024b). The validation of prediction performances is usually based on databases Jaume et al. (2024a); Chen et al. (2024a) with paired spatial transcriptomics and H&E images.

Sample Difficulty. The measurement of sample difficulty can come from either task-specific designs and models Agarwal et al. (2022); Baldock et al. (2021); Zhu et al. (2024), or from pre-trained models Cui et al. (2023). Previously, researchers focused on uncertainty regularization as an effective approach to reducing the overfitting and over-confidence problems in the training stage of the classifier. In the classification problem, most of them are based on the modification of loss functions, for example, Focal loss Liu et al. (2020), L_p norm Joo & Chung (2021), Poly loss (Poly) Leng et al. (2022), Entropy Regularization (ER) Mnih (2016), Weighted Entropy Regularization (WER), and Weighted Poly Loss (WPoly) Cui et al. (2023) are based on adding regularization terms in the loss function to improve the optimization process. The weight could come from the pre-defined distance used to measure the difficulty level of training samples. Other methods such as label smoothing Müller et al. (2019) and correctness ranking loss (CRL) Moon et al. (2020) modify the labels to penalize the samples with the highest prediction confidence, which could be potential solutions. In the regression problem, ordinary entropy (OE) Zhang et al. (2023) is developed to regularize neural networks for handling regression-based tasks inspired by the phenomenon that formatting regression problems as classification problems is helpful. We also consider modified loss functions such as Huber loss Huber (1992), which can contribute for reducing the drawbacks caused by underfitting.

3 Method

Problem Definition. In this paper, we are given a histopathology dataset $\mathcal{D} = \{\mathbf{x}_i, y_i\}_{i=1}^n$, where $\mathbf{x}_i$ represents an m-dimensional feature vector extracted from PFMs for the i-th whole-slide image (WSI) or patch (which is an image extracted from WSI based on certain rules) and y_i represents the corresponding targets for prediction, i.e., disease states for the classification task (y_i is a scalar) or gene expression levels (y_i is a vector as we have multiple genes to predict) for regression task. For the classification task, we train a classifier C_θ based on the training dataset, and may observe sample $\mathbf{x}_d$ whose predicted labels mismatch with the observed label ($C_\theta(\mathbf{x}_d) \neq y_d$). These samples can be treated as difficult samples. Our target is to identify difficult samples and further improve model performances by correctly predicting these samples in the training stage as many as possible. The formal definition of sample difficulty analysis for the regression problem is similar, and the label of each sample can be computed by discretizing y into different bins, while the mismatched samples are still difficult samples under this context.

Overview. USD starts from estimating the sample difficulty levels based on image features extracted from pre-trained base models such as PFMs. We then leverage the sample difficulty to regularize the model outputs in the training stage, as a more difficult sample should be assigned to having a higher weight. To effectively predict gene expression levels based on spatial transcriptomics and paired sets of patches, we consider both

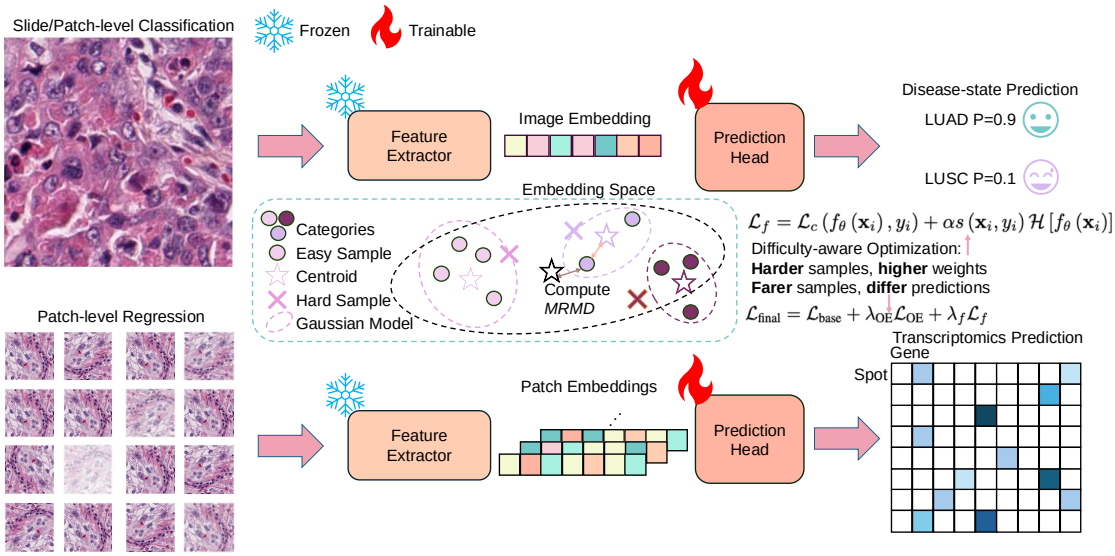

Figure 2: Illustration of USD's pipeline. We accept either slide-level information or patch-level information as input and incorporate the estimated sample difficulty from prior in the training process by reconstructing the target of optimization. By default, PFMs are frozen and only used for extracting image embeddings, while task-specific adapters are trained for different datasets.

sample difficulty and the relationship between expression-level similarity and feature-level similarity. We visualize USD in Figure 2.

Foundation Models as Feature Extractor. We first utilize pre-trained PFMs to embed the images into feature space, which can provide better representations discussed in the previous work Cui et al. (2023). In summary, PFMs are generally trained to ignore low-level information (e.g., class labels) and prioritize whole-image level information rather than low-level image statistics. Moreover, PFMs are trained with more diverse data, which can better learn and extract the intrinsic features of input images and remove noisy information. Therefore, the generated features will be helpful to estimate training difficulty in a robust space and support USD to perform downstream applications.

Estimating Sample Difficulty with Prior Knowledge. For training dataset $\mathcal{D}_{train} = \{\mathbf{x}_i, y_i\}_{i=1}^{n_1}$, we first derive the relative Mahalanobis distance (RMD) as the sample difficulty score, which has been shown as a more powerful approach to detect difficult samples Cui et al. (2023). The computation of RMD is introduced later and it can measure the distribution-level difference to define easy samples and difficult samples. For samples with $y_i = k$, we fit a Gaussian model of the set of features $\{\mathbf{x}_i\}$ as $G(\mathbf{x}_i)$. The model can be computed based on:

$$
\begin{aligned}
\mathbb{P}(G_k(\mathbf{x}) \mid y = k) &= \mathcal{N}\left(G_k(\mathbf{x}) \mid \boldsymbol{\mu}_k, \Sigma\right), \\
\boldsymbol{\mu}_k &= \frac{1}{N_k} \sum_{i:y_i=k} G_k\left(\mathbf{x}_i\right), \\
\Sigma &= \frac{1}{N} \sum_k \sum_{i:y_i=k} \left(G_k\left(\mathbf{x}_i\right) - \boldsymbol{\mu}_k\right)\left(G_k\left(\mathbf{x}_i\right) - \boldsymbol{\mu}_k\right)^\top,
\end{aligned}
\tag{1}
$$

where $\boldsymbol{\mu}_k$ represents the mean vector and Σ represents the sample covariance matrix, N_k represents the samples belonging to class k, and G_k represents the Gaussian model for the class k. Similarly, considering all training samples as a background, we can fit a Gaussian model G_b:

$$
\begin{aligned}
\mathbb{P}(G_b(\mathbf{x})) = \mathcal{N}\left(G_b(\mathbf{x}) \mid \boldsymbol{\mu}_b, \Sigma_b\right), \boldsymbol{\mu}_b &= \frac{1}{N} \sum G_b\left(\mathbf{x}_i\right), \\
\Sigma_b &= \frac{1}{N} \sum \left(G_b\left(\mathbf{x}_i\right) - \boldsymbol{\mu}_b\right)\left(G_b\left(\mathbf{x}_i\right) - \boldsymbol{\mu}_b\right)^\top,
\end{aligned}
\tag{2}
$$

where N represents the number of samples used for fitting, and $\boldsymbol{\mu}_b$ and Σ_b represent the estimated mean and covariance matrix for all samples used for training.

The high-level idea is to have a metric that can reflect both the sample similarity within the same label as well as sample difference across different labels. For example, an easy-classified sample should be close to the mean vector of assigned labels (representative) and far from the mean vectors of observed samples (discriminative), estimated based on the Gaussian model. Therefore, for one sample $\mathbf{x}_i$ with label $y_i = k$, we can define its RMD based on the difference of MD computed based on G_k and G_b as:

$$\mathcal{RMD}_k\left(\mathbf{x}_i, k\right) = \mathcal{MD}_k\left(\mathbf{x}_i, k\right) - \mathcal{MD}_b\left(\mathbf{x}_i\right), \tag{3}$$

where $\mathcal{MD}_k$ and $\mathcal{MD}_b$ represent the Mahalanobis distance computed based on samples and different clustering centroid. The formal computation of $\mathcal{MD}$ is:

$$\begin{aligned} \mathcal{MD}_k\left(\mathbf{x}_i, k\right) &= -\left(G_k\left(\mathbf{x}_i\right) - \boldsymbol{\mu}_k\right)^\top \Sigma^{-1}\left(G_k\left(\mathbf{x}_i\right) - \boldsymbol{\mu}_k\right), \\ \mathcal{MD}_b\left(\mathbf{x}_i\right) &= -\left(G_b\left(\mathbf{x}_i\right) - \boldsymbol{\mu}_b\right)^\top \Sigma_b^{-1}\left(G_b\left(\mathbf{x}_i\right) - \boldsymbol{\mu}_b\right). \end{aligned} \tag{4}$$

However, fitting a model based on training datasets still has the risk of estimating wrong difficulty levels. For example, there exist samples with low $\mathcal{RMD}$ with misclassified results and samples with high $\mathcal{RMD}$ but correctly assigned labels based on a simple linear classifier, shown in Appendix 6.2. Moreover, the consistency of sample difficulty is also important in the estimation, and Appendix 6.2 shows that using different splits do not change the proportion of difficult samples significantly. Therefore, we estimate a prior from several fitted logistic regression (LR) models based on the cross-validation approach. For the given training dataset $\mathcal{D}_{train}$, we split the dataset into q folds based on cross-validation and fit q LR models. By collecting all the samples wrongly classified by these models, we can have a list containing n_q difficult samples derived from simple classifiers, denoted as $\{\mathbf{x}_i\}_{i=1}^{n_q}$, which can be further converted into the indicator weight w. This approach can also be used to determine whether we need to fit a neural-network-based classifier for the given problem. Moreover, we assign the maximal $\mathcal{RMD}$ for these samples, and the modified distance is defined as $\mathcal{MRMD}$ with the indicator weight. Therefore, if $w_{\mathbf{x}_i} = 1$, the $\mathcal{MRMD}$ for sample $\mathbf{x}_i$ is defined as:

$$\mathcal{MRMD}_{y_i}\left(\mathbf{x}_i, y_i\right) = \max_j \mathcal{RMD}_{y_j}\left(\mathbf{x}_j, y_j\right), \tag{5}$$

otherwise $\mathcal{MRMD}$ is the same as the pre-computed $\mathcal{RMD}$. When we train the model to classify sample $\mathbf{x}_i$, we regularize the classification loss function by treating $\mathcal{MRMD}$ as adaptive weights:

$$\begin{aligned} \mathcal{L}_f &= \mathcal{L}_c\left(f_\theta\left(\mathbf{x}_i\right), y_i\right) + \alpha s\left(\mathbf{x}_i, y_i\right)\mathcal{H}\left[f_\theta\left(\mathbf{x}_i\right)\right], \\ s\left(\mathbf{x}_i, y_i\right) &= \frac{\exp\left(\mathcal{MRMD}\left(\mathbf{x}_i, y_i\right)/T\right)}{\max_j\left\{\exp\left(\mathcal{MRMD}\left(\mathbf{x}_j, y_j\right)/T\right\} + \epsilon\right.}, \end{aligned} \tag{6}$$

where L_c represents the cross-entropy loss, $f_\theta(\cdot)$ represents the classifier, $\mathcal{H}(\cdot)$ represents the regularized element (it can be either negative entropy or poly loss), and $s(\cdot,\cdot)$ represents the difficulty weight. α is the weight used for loss balancing, T is the temperature parameter to control the shape of weight distribution, and ϵ represents a tiny value to avoid numerical errors. In the real application of USD to improve classification, for stable training, we normalize the distance $\mathcal{MRMD}(\mathbf{x}_i, y_i)$ into the range of $(0, 1)$. The regularized loss $\mathcal{L}_f$ can be trained with Adam Kingma (2014) optimizer. During the training stage, the difficulty score is min-max normalized to keep the stability of training. If we do not detect wrongly classified samples in this stage, our method degrades to no-prior mode. We have also provided a systemic comparison between USD and $\mathcal{RMD}$ in Appendix 6.2.

Estimating Sample Difficulty for Regression Problems. Previous research Pintea et al. (2023) has demonstrated that reconsidering regression problems in computer vision as classification problems can always boost model performance. Therefore, the sample difficulty of continuous labels can be estimated after transferring the continuous targets as discrete targets, for example, based on clustering methods after batch effect correction Korsunsky et al. (2019); Tran et al. (2020) or Bins-Discretizer methods Pedregosa et al.

(2011). Therefore, assuming we have the transferring function $t(\cdot)$ and the discrete labels computed based on $k = t(\mathbf{y}_i)$, the difficulty of updated sample $(\mathbf{x}_i, k)$ can be defined as:

$$\mathcal{RMD}_k\left(\mathbf{x}_i, k\right) = \mathcal{MD}_k\left(\mathbf{x}_i, k\right) - \mathcal{MD}_b\left(\mathbf{x}_i\right), \tag{7}$$

where the computation of $\mathcal{MRMD}_k\left(\mathbf{x}_i, k\right)$ is the same as steps used in the classification task.

The number of clusters and bins is tuned based on maximizing the Average Silhouette Width (ASW) score Pedregosa et al. (2011). The computation process of $\mathcal{MD}_k(\cdot,\cdot)$ and $\mathcal{MD}_b(\cdot)$ is the same as the approaches used in classification. Similarly, $\mathcal{MRMD}(\cdot,\cdot)$ can also be computed based on LR with features from PFMs as inputs and discrete labels as targets.

Learning Sample Difficulty for a General Purpose. When considering the loss of (multi-target) regression-based problems, we propose a new correlation-aware and difficulty-aware loss function for gene expression prediction. Most of the previous work relied on minimizing the mean squared error (MSE$(\cdot,\cdot)$) of multiple genes between observed expression levels $\mathbf{y}_i$ for spot i and predicted expression levels $\hat{\mathbf{y}}_i$. However, this approach only considers the global cost but ignores the fine-grained differences across spots and genes. Therefore, we first introduced the designed PCCMSE loss, which is the combination of MSE loss, spot-level Pearson correlation coefficient (PCC) loss, and gene-level PCC loss. Its definition is:

$$\mathcal{L}_{\text{base}} = \text{MSE}(\mathbf{y}, \hat{\mathbf{y}}) - \text{PCC}(\mathbf{y}, \hat{\mathbf{y}}) - \text{PCC}(\mathbf{y}^\top, \hat{\mathbf{y}}^\top). \tag{8}$$

Furthermore, inspired by Zhang et al. (2023), we also introduce the Ordinary Entropy loss function (OE) in the optimization process, which can reduce the entropy in the training process by balancing the tightness and diversity of feature space. The second term of our loss function is defined as:

$$\begin{aligned}\mathcal{L}_{\text{OE}} = &-\frac{1}{M(M-1)}\sum_{i=1}^{M}\sum_{j\neq i} w_{ij}\left\|\mathbf{z}_{c_i} - \mathbf{z}_{c_j}\right\|_2 \\ &+ \frac{1}{M_b}\sum_{i=1}^{M_b}\left\|\mathbf{z}_i - \mathbf{z}_{c_i}\right\|_2,\end{aligned} \tag{9}$$

where $w_{ij} = \left\|\mathbf{y}_i - \mathbf{y}_j\right\|_2$ ensures that samples with larger distances in the expression space will receive a large penalty. Here c_i and c_j represent the centers in the feature space of samples i and j, and $\mathbf{z}_i$ represents the embeddings from the outputs of the last encoder layer for the i-th sample. M represents the number of centers and M_b represents the number of samples in the given batch b. Finally, in our case, each feature is its center because of the expression difference, so we have $\left\|\mathbf{z}_i - \mathbf{z}_{c_i}\right\|_2 = 0$.

We finally incorporate the difficulty-aware loss function inspired by the classification problem in equation equation 6. We can make categorization for given samples and compute sample difficulty to provide regularization, and thus, the renewed $\mathcal{L}_f$ for regression task with transformed prediction value v:

$$\begin{aligned}\mathcal{L}_{f(reg)} &= \mathcal{L}_c\left(f_\theta\left(\mathbf{x}_i\right), v_i\right) + \alpha s\left(\mathbf{x}_i, v_i\right)\mathcal{H}\left[f_\theta\left(\mathbf{x}_i\right)\right], \\ s\left(\mathbf{x}_i, v_i\right) &= \frac{\exp\left(\mathcal{MRMD}\left(\mathbf{x}_i, v_i\right)/T\right)}{\max_j\left\{\exp\left(\mathcal{MRMD}\left(\mathbf{x}_j, v_j\right)/T\right\} + \epsilon\right.}.\end{aligned} \tag{10}$$

Therefore, our final loss function used in USD can be represented as:

$$\mathcal{L}_{\text{final}} = \mathcal{L}_{\text{base}} + \lambda_{\text{OE}}\mathcal{L}_{\text{OE}} + \lambda_f\mathcal{L}_{f(reg)}, \tag{11}$$

where $\lambda_{\text{OE}}, \lambda_f$ are hyper-parameters used to control the balance of the last two loss function terms. All the hyper-parameters are tuned to the optimized version based on the model performance on the validation dataset for both baseline and proposed methods.

4 Experiment

4.1 Setup

Datasets. For the disease-state classification problem, we consider three datasets covering different sub-tasks. We perform experiments of our proposed method and baseline methods for disease sub-type classification based on TCGA LUSC-LUAD (TCGA) Weinstein et al. (2013) dataset, and perform experiments for disease-state classification based on CAMELYON16 Bejnordi et al. (2017) and PANDA datasets Bulten et al. (2022). PANDA is designed as a multi-classification problem with six classes. TCGA LUSC-LUAD is a slide-level small-scale dataset and the latter two are slide-level large-scale datasets. We generate training/validation/testing samples for these three datasets randomly. Label distributions are summarized in Appendix 6.4. For the spatial transcriptomics prediction as a patch-level task, we consider eight datasets named by the source diseases/tissues (IDC, READ, PRAD, LYMPH_IDC, COAD, CCRCC, Brain, and Skin) from the HEST-1k database Jaume et al. (2024a) and STImage-1K4M database Chen et al. (2024a). The highly variable genes used for training and prediction are pre-defined in these datasets. Each dataset corresponds to one cancer or tissue type, and we filter the disease dataset whose number of batches is lower than three, which is the minimal number we need to split the whole dataset into training/validation/testing samples.

Evaluations. For the classification task, we select metrics Pedregosa et al. (2011) including Accuracy (Acc), Balanced Accuracy (Bacc), Kappa coefficient (Kappa), Weighted-F1 score (wF1), Area Under the Receiver Operating Characteristic curve score (AUROC), and Expected Calibration Error (ECE) Kuleshov & Liang (2015). The higher the better for all metrics except ECE. Lower ECE represents better calibrating confidence. We did not include AUROC for evaluating the multi-class classification problem. For the regression task, we select metrics including spot-level PCC (SPCC), gene-level Pearson Correlation Coefficients (GPCC), and Mean Squared Error (MSE). The higher the better for all metrics except MSE. All metrics are widely used in the related work Chen et al. (2024b); Jia et al. (2024); Liu et al. (2025a) of classification and regression tasks.

Baseline Models. We have considered base models including UNI v1 Chen et al. (2024b), UNI v2 Chen et al. (2024b), GigaPath Xu et al. (2024a), and ResNet 50 He et al. (2016) for generating image features. We also considered Multi-Instance Learning methods (e.g. ABMIL Ilse et al. (2018)) as baselines, discussed in Appendix 6.11. ABMIL is a weaker baseline. Our selection criteria are based on the related benchmarking analyses in this task Jaume et al. (2024a); Lee et al. (2024a); Zhang et al. (2025); Vaidya et al. (2025), and training strategies are inherited from Cui et al. (2023). We exclude image-text-based PFMs to avoid data leakage. For disease-state classification, we consider LS Müller et al. (2019), L_1 Joo & Chung (2021), Focal Mukhoti et al. (2020), Poly Leng et al. (2022), ER Pereyra et al. (2017), CE Mannor et al. (2005), WER Cui et al. (2023), and WPoly Cui et al. (2023) as baseline models, which are widely used in related work. For gene expression prediction, we consider MSE Loss Wang & Bovik (2009), Huber Loss Huber (1992), and PCCMSE Loss as baseline models. Here MSE Loss is the most frequently used loss function in this task. Details of selected baselines can be found in Appendix 6.5.

Implementation Details. We implement our method using a single H200 NVIDIA GPU and adopt mini-batch Adam training with a batch size proportion to data scale (32 for the dataset with $n_{\text{samples}} < 1000$ and 512 for the dataset with $n_{\text{samples}} > 1000$), and the batch size is also determined under the consideration of the GPU memory usage. We utilize PyTorch-lightning Falcon (2019) to train the model and evaluate different baselines accordingly. All the spatial transcriptomic data are normalized by standard pipeline from Scanpy Wolf et al. (2018). For tuning other hyper-parameters, please refer Appendix 6.6. All baseline methods are tuned to their optimal stage for a fair comparison. For running time and memory usage, please refer Appendix 6.7.

4.2 Experimental Results

Disease State Classification. We select Acc and AUROC for evaluating the dataset with binary labels, while Acc and wF1 are presented for evaluating the dataset with multiple labels, summarized in Table 1. We also provide tables with full metrics, which are listed in Appendix 6.8. We first consider LR as a simple baseline for assessing the necessity of performing training with non-linear models based on Appendix 6.9, which shows that PFMs with USD are always better than LR across different datasets. Overall, if we consider

Datasets	Metrics	Base	Methods										
			LS	L_1	Focal	Poly	ER	CE	WER	WPoly	**USD (ER)**	**USD (Poly)**	Best Method
TCGA	ACC (↑)	UNI v1	0.420	0.923	0.913	0.927	**0.933**	0.913	**0.933**	0.923	**0.933**	0.923	UNIv2+USD (ER)
		UNI v2	0.520	0.960	0.933	0.930	0.963	0.923	**1.000**	0.920	**1.000**	0.920	
		GigaPath	0.510	0.647	0.603	0.760	0.697	0.737	0.677	**0.767**	0.677	**0.767**	
		ResNet 50	0.517	0.517	0.653	0.637	0.520	0.643	0.640	**0.690**	0.627	0.680	
	AUROC (↑)	UNI v1	0.446	0.986	0.987	0.986	**0.994**	0.986	0.994	0.989	**0.994**	0.989	UNIv2+USD (ER)
		UNI v2	0.543	**1.000**	**1.000**	**1.000**	0.997	**1.000**	**1.000**	**1.000**	**1.000**	**1.000**	
		GigaPath	0.570	0.742	0.838	0.859	0.877	0.866	**0.898**	0.891	**0.898**	0.891	
		ResNet 50	0.545	0.517	0.704	0.697	0.568	0.696	0.664	0.721	0.677	**0.731**	
CAMELYON16	ACC (↑)	UNI v1	0.494	0.715	0.715	0.726	0.732	0.747	0.724	0.724	0.741	**0.756**	UNIv1+USD (Poly)
		UNI v2	0.450	0.574	**0.585**	0.559	0.553	0.559	0.538	0.518	0.562	0.550	
		GigaPath	0.491	0.491	0.468	0.459	0.482	**0.497**	0.488	0.462	0.491	0.485	
		ResNet 50	0.541	0.535	0.529	0.524	0.497	0.521	0.456	0.535	**0.585**	0.553	
	AUROC (↑)	UNI v1	0.536	0.828	0.821	0.832	0.831	0.829	0.821	0.820	0.812	**0.834**	UNIv1+USD (Poly)
		UNI v2	0.463	0.752	0.690	0.738	0.738	0.724	0.701	0.713	**0.753**	0.739	
		GigaPath	0.519	**0.649**	0.593	0.619	0.610	0.610	0.592	0.575	0.643	0.661	
		ResNet 50	0.524	0.725	0.720	0.719	0.719	0.725	0.515	0.712	**0.730**	0.703	
PANDA	ACC (↑)	UNI v1	0.147	0.489	0.484	0.490	0.474	0.471	0.485	0.485	**0.495**	0.494	UNIv1+USD (ER)
		UNI v2	0.165	0.479	0.479	**0.489**	0.480	0.479	0.474	0.485	0.488	0.468	
		GigaPath	0.182	0.468	0.459	0.470	0.460	0.465	0.460	0.466	**0.473**	0.453	
		ResNet 50	0.178	0.417	0.437	0.440	0.437	**0.439**	0.429	0.438	0.430	0.431	
	wF1 (↑)	UNI v1	0.099	0.458	0.468	0.467	0.445	0.446	0.467	0.469	**0.479**	0.478	UNIv1+USD (ER)
		UNI v2	0.165	0.479	0.479	**0.489**	0.480	0.479	0.474	0.485	0.488	0.468	
		GigaPath	0.171	0.437	0.435	0.445	0.438	0.446	0.428	0.440	**0.455**	0.424	
		ResNet 50	0.174	0.342	**0.416**	0.413	0.415	**0.416**	0.403	0.413	0.397	0.404	

Table 1: Benchmarking results across base models and training strategies for classification tasks. We reported the average scores for each method from five random seeds, and the information on standard deviation can be found in Appendix 6.8. Our proposed method and the best score are boldfaced.

evaluating the training strategies based on different PFMs (including 12 combinations), USD achieves the highest performance in 75.0% choices evaluated by AUROC or wF1 and 53.8% choices evaluated by Acc, demonstrating the consistent improvement of USD. Furthermore, the ER mode of USD is more helpful for handling datasets with complicated structures (e.g., multi-label classification) and can also reduce the uncertainty when making the decision, reflected by the lower ECE. If we focus on a specific dataset such as TCGA, the best combination, UNI v2 and USD with ER mode, can surpass the second-best combination by 3.8%. The Poly mode of USD is more suitable for datasets with simpler structures. Both of the proposed modes have low standard deviation, shown in Appendix 6.8. The improvement of USD versus the 2nd-best method is also significant validated by the Wilcoxon Rank-sum test, whose p-value is 1.25e-4 across base models and datasets. We also demonstrate the robustness of USD under imbalanced or noisy labels, shown in Appendix 6.4. As a result, USD acts as an efficient solution to improve the accuracy of image classification on a wide range of problem types and data, and can be easily integrated into more training pipelines.

Gene Expression Prediction. We first select the most promising PFM to form the base model for predicting spatial transcriptomics based on PCCMSE Loss. According to the Appendix 6.8, UNI v2 is the best option for predicting gene expression levels from patches, so we conduct main experiments based on this model to reduce the cost of generating path-level embeddings for each dataset, estimating the sample difficulty, and training different models for expression prediction. According to Table 2, MSE Loss and Huber Loss generally perform worse than PCCMSE Loss, reflected in the lower SPCC score and GPCC score, as well as higher MSE, on average. USD also surpasses state-of-the-art training framework, DeepPT Hoang et al. (2024), discussed in Appendix 6.10. Moreover, USD achieves the highest SPCC score in 75% datasets and the highest GPCC score in 50% datasets. Compared with the second-best method in the selected metrics, USD makes an average improvement by 3.2% for SPCC and 1.8% for GPCC. If we compare USD with MSE Loss, which is a more generally used loss function in this task, we can improve the model performance by 62.2% at most for GPCC in the Brain dataset. USD also has low variance, validated by the table with information of the standard deviation. Therefore, USD can participially predict gene expression levels higher than the baselines based on the cross-gene evaluation setting, which is closer to the practical applications of gene expression analysis, such as the detection of differential expression gene Kiselev et al. (2019); Song et al. (2023b) and the selection of cell-type-specific marker genes Pullin & McCarthy (2024). The improvement of USD versus the 2nd-best method is also significant validated by the Wilcoxon Rank-sum test, whose p-value is 2.6e-3 across base models and datasets.

Metrics	Methods	Datasets and Rank									
		IDC	READ	PRAD	LYMPH_IDC	COAD	CCRCC	Brain	Skin	Average	Avg Rank
SPCC (↑)	MSE Loss	0.581	0.332	**0.691**	0.103	0.621	0.373	0.602	0.400	0.463	3.78
	Huber Loss	0.589	0.322	0.684	0.090	**0.626**	0.369	0.605	0.393	0.460	4.11
	PCCMSE Loss	0.588	0.360	0.687	0.049	0.621	0.383	0.615	0.401	0.463	3.44
	PCCMSE+OE	**0.591**	0.359	0.689	0.127	0.624	0.381	0.617	0.406	0.474	2.22
	USD (ER)	0.589	**0.381**	0.689	**0.129**	0.622	**0.386**	**0.618**	**0.409**	**0.478**	**1.44**
GPCC (↑)	MSE Loss	0.389	0.190	0.132	0.242	0.565	0.264	0.095	0.237	0.264	4.11
	Huber Loss	0.390	0.166	0.134	**0.250**	**0.568**	0.251	0.102	0.198	0.257	3.67
	PCCMSE Loss	**0.400**	0.271	0.134	0.219	0.562	**0.284**	0.133	**0.266**	0.284	2.78
	PCCMSE+OE	0.399	0.271	0.135	0.234	0.567	0.266	0.151	0.264	0.286	2.67
	USD (ER)	**0.400**	**0.283**	**0.138**	0.236	0.565	0.273	**0.154**	0.265	**0.289**	**1.78**
MSE (↓)	MSE Loss	2.825	0.264	**0.293**	0.845	0.959	0.491	0.281	1.561	0.940	2.78
	Huber Loss	2.812	**0.228**	0.301	0.864	0.969	0.499	**0.279**	1.578	0.941	**2.00**
	PCCMSE Loss	2.748	0.242	**0.293**	**0.769**	0.958	**0.486**	0.285	1.578	**0.920**	3.78
	PCCMSE+OE	**2.718**	0.242	0.295	0.859	**0.955**	0.487	0.293	1.516	0.921	3.44
	USD (ER)	2.754	0.269	0.294	0.857	0.957	0.492	**0.279**	**1.481**	0.923	3.00

Table 2: Benchmarking results for the regression task. We report the average scores (Average) for each method from five random seeds and average rank (Avg Rank) by averaging each method's rank across different datasets. The information on standard deviation can be found in Appendix 6.8. USD and the score with the best value are boldfaced, and lower rank represents a better method.

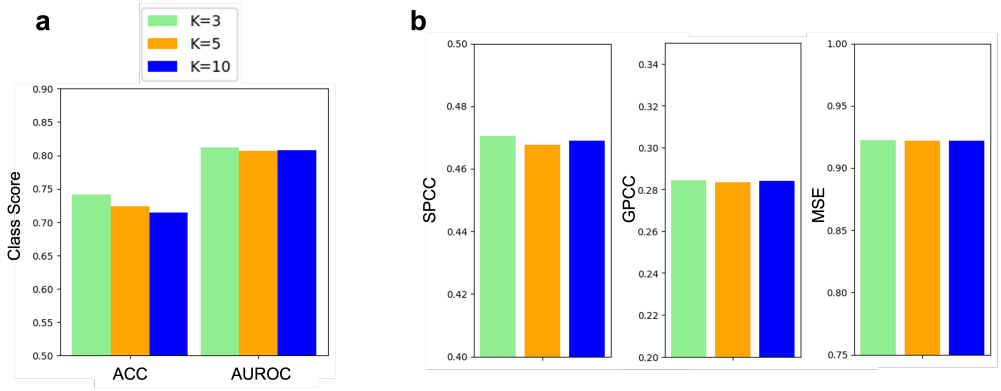

Figure 3: Results of choosing different K. (a) represents the results performed for the classification task. (b) represents the results performed for the regression task.

4.3 Analysis

Insights from Analyzing Factors Affecting Image Classification. To estimate the sample difficulty with prior, we need to run K-fold cross-validation to collect the samples that are wrongly predicted by a simple linear predictor. By adjusting different K, we have various sample lists with different lengths. To determine a suitable K and demonstrate the robustness of our method, we examine different K based on the CAMELYON16 dataset with base model UNI v1. According to Figure 3 (a), increasing K may slightly reduce model performance, which shows that our training strategy expects a relatively smaller K to generate difficult sample sets. Moreover, very large K requires longer training time, and thus we finally fix $K = 3$ for all datasets. We also consider the options of input type with different modes, the necessity of dropping the difficult samples or fine-tuning the base model and prediction head together, and the options of computing sample difficulty, discussed in Appendix 6.11. These variations cannot make improvement.

Lessons from Analyzing Factors Affecting Gene Expression Prediction. In the regression task, based on Figure 3 (b), adjusting K will not affect model performance too much, and thus USD is very robust to K in the gene expression prediction setting. We have included a similar study for the cluster number with all datasets in Appendix 6.12. Furthermore, we perform ablation studies to investigate the contribution

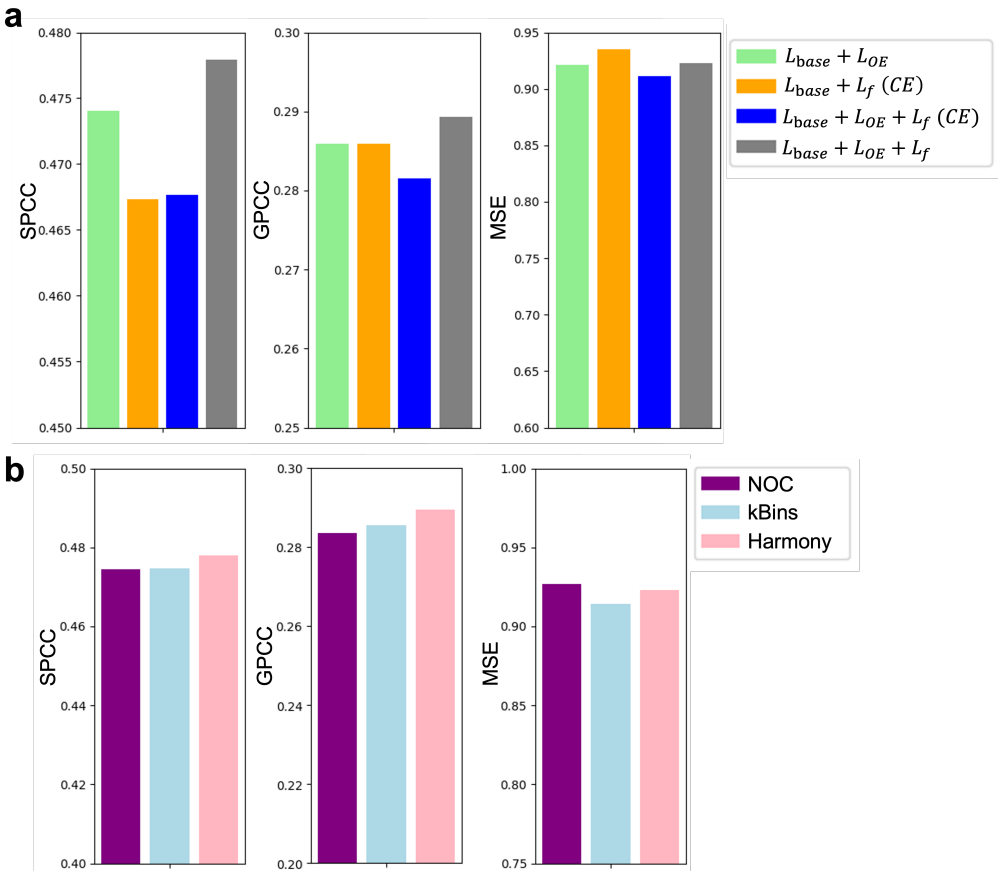

Figure 4: Ablation tests for the regression task. (a) represents the results under different components of final loss. The mode *CE* means using cross entropy as the classification loss. Raw scores can be foun in Table 27. (b) represents the results under different batch effect correction strategies.

of different loss function components, summarized in Figure 4 (a). According to this figure, our final loss function $\mathcal{L}_{\text{final}}$ has the highest SPCC and GPCC scores, while its MSE is close to the best method. Moreover, we find that incorporating the term $\mathcal{L}_{\text{OE}}$ can help us better learn the cell-level and gene-level correlations while adding the term $\mathcal{L}_f$ regularized by the sample difficulty helps us reducing the average error between predicted and observed expression levels. This conclusion matches with previous studies arguing that utilizing classification loss can reduce the MSE for the regression task. If we do not consider incorporating sample difficulty and use cross entropy (CE) to compute the classification loss, we cannot achieve improvement. We also consider the approaches to reduce batch effect in the expression space, including Harmony, kBins, and no correction mode (NoC), and the results are summarized in Figure 4 (b). Correcting batch effect can improve model performance. Running Harmony or KBins can make the correlation smoother and reduce the batch effect in the relationship of SPCC and difficulty, shown in Figure 5. The comparisons of different modes and base models are summarized in Appendices 6.13 and 6.14.

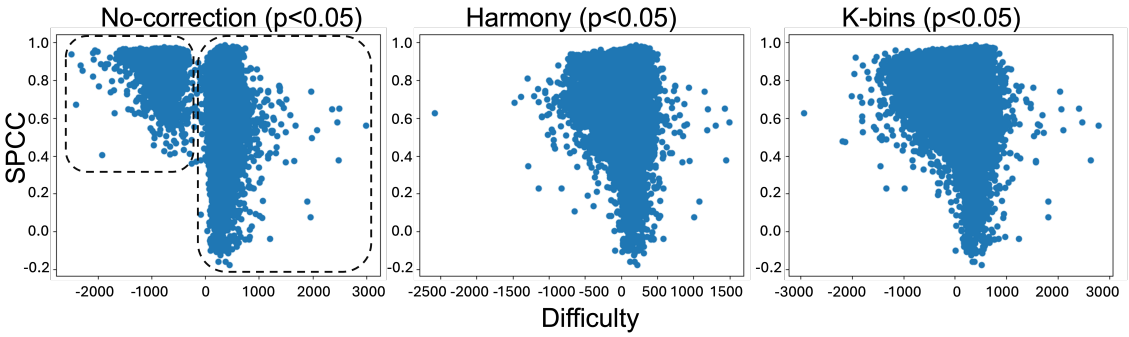

Figure 5: Relationship between sample difficulty and SPCC based on adjusting different batch effect correction strategies. The SPCC is computed based on the training dataset.

5 Conclusion

This paper investigates a clinical-associated problem of estimating the slide-level or patch-level training difficulty to boost model performances targeting two typical tasks in histopathology image analysis, including the classification of disease states and the prediction of spatial transcriptomics. We introduced a novel framework to estimate the sample difficulty from prior information. Moreover, under the concept of unified setting, we intend to point out that regression setting should be interpreted as an approximation that enables unified evaluation, rather than as a fully faithful characterization of continuous prediction problems. In the future, we will revise the current limitations, extend our applications to more scenarios, such as sample-difficulty-based foundation model pre-training.

References

Chirag Agarwal, Daniel D'souza, and Sara Hooker. Estimating example difficulty using variance of gradients. In *Proceedings of the IEEE/CVF Conference on Computer Vision and Pattern Recognition*, pp. 10368–10378, 2022.

Shaimaa Al-Janabi, André Huisman, and Paul J Van Diest. Digital pathology: current status and future perspectives. *Histopathology*, 61(1):1–9, 2012.

Anonymous. Predicting spatial transcriptomics from histology images via biologically informed flow matching. In *Submitted to The Thirteenth International Conference on Learning Representations*, 2024. URL `https://openreview.net/forum?id=sYrdb3mhM4`. under review.

John Arevalo, Ellen Su, Jessica D Ewald, Robert van Dijk, Anne E Carpenter, and Shantanu Singh. Evaluating batch correction methods for image-based cell profiling. *Nature Communications*, 15(1):6516, 2024.

Erick Armingol, Adam Officer, Olivier Harismendy, and Nathan E Lewis. Deciphering cell–cell interactions and communication from gene expression. *Nature Reviews Genetics*, 22(2):71–88, 2021.

Robert Baldock, Hartmut Maennel, and Behnam Neyshabur. Deep learning through the lens of example difficulty. *Advances in Neural Information Processing Systems*, 34:10876–10889, 2021.

Babak Ehteshami Bejnordi, Mitko Veta, Paul Johannes Van Diest, Bram Van Ginneken, Nico Karssemeijer, Geert Litjens, Jeroen AWM Van Der Laak, Meyke Hermsen, Quirine F Manson, Maschenka Balkenhol, et al. Diagnostic assessment of deep learning algorithms for detection of lymph node metastases in women with breast cancer. *Jama*, 318(22):2199–2210, 2017.

Kaustav Bera, Kurt A Schalper, David L Rimm, Vamsidhar Velcheti, and Anant Madabhushi. Artificial intelligence in digital pathology—new tools for diagnosis and precision oncology. *Nature reviews Clinical oncology*, 16(11):703–715, 2019.

Wouter Bulten, Kimmo Kartasalo, Po-Hsuan Cameron Chen, Peter Ström, Hans Pinckaers, Kunal Nagpal, Yuannan Cai, David F Steiner, Hester Van Boven, Robert Vink, et al. Artificial intelligence for diagnosis and gleason grading of prostate cancer: the panda challenge. *Nature medicine*, 28(1):154–163, 2022.

Jiawen Chen, Muqing Zhou, Wenrong Wu, Jinwei Zhang, Yun Li, and Didong Li. STimage-1k4m: A histopathology image-gene expression dataset for spatial transcriptomics. In *The Thirty-eight Conference on Neural Information Processing Systems Datasets and Benchmarks Track*, 2024a. URL `https://openreview.net/forum?id=iTyOWtcCU2`.

Richard J Chen, Tong Ding, Ming Y Lu, Drew FK Williamson, Guillaume Jaume, Andrew H Song, Bowen Chen, Andrew Zhang, Daniel Shao, Muhammad Shaban, et al. Towards a general-purpose foundation model for computational pathology. *Nature Medicine*, 30(3):850–862, 2024b.

Peng Cui, Dan Zhang, Zhijie Deng, Yinpeng Dong, and Jun Zhu. Learning sample difficulty from pre-trained models for reliable prediction. *Advances in Neural Information Processing Systems*, 36:25390–25408, 2023.

Jia Deng, Wei Dong, Richard Socher, Li-Jia Li, Kai Li, and Li Fei-Fei. Imagenet: A large-scale hierarchical image database. In *2009 IEEE conference on computer vision and pattern recognition*, pp. 248–255. Ieee, 2009.

Tong Ding, Sophia J Wagner, Andrew H Song, Richard J Chen, Ming Y Lu, Andrew Zhang, Anurag J Vaidya, Guillaume Jaume, Muhammad Shaban, Ahrong Kim, et al. Multimodal whole slide foundation model for pathology. *arXiv preprint arXiv:2411.19666*, 2024.

Alexey Dosovitskiy, Lucas Beyer, Alexander Kolesnikov, Dirk Weissenborn, Xiaohua Zhai, Thomas Unterthiner, Mostafa Dehghani, Matthias Minderer, Georg Heigold, Sylvain Gelly, Jakob Uszkoreit, and Neil Houlsby. An image is worth 16x16 words: Transformers for image recognition at scale. In *International Conference on Learning Representations*, 2021. URL `https://openreview.net/forum?id=YicbFdNTTy`.

William A Falcon. Pytorch lightning. *GitHub*, 3, 2019.

Kaiming He, Xiangyu Zhang, Shaoqing Ren, and Jian Sun. Deep residual learning for image recognition. In *Proceedings of the IEEE conference on computer vision and pattern recognition*, pp. 770–778, 2016.

Danh-Tai Hoang, Gal Dinstag, Eldad D Shulman, Leandro C Hermida, Doreen S Ben-Zvi, Efrat Elis, Katherine Caley, Stephen-John Sammut, Sanju Sinha, Neelam Sinha, et al. A deep-learning framework to predict cancer treatment response from histopathology images through imputed transcriptomics. *Nature Cancer*, pp. 1–13, 2024.

Zhi Huang, Federico Bianchi, Mert Yuksekgonul, Thomas J Montine, and James Zou. A visual–language foundation model for pathology image analysis using medical twitter. *Nature medicine*, 29(9):2307–2316, 2023.

Peter J Huber. Robust estimation of a location parameter. In *Breakthroughs in statistics: Methodology and distribution*, pp. 492–518. Springer, 1992.

Maximilian Ilse, Jakub Tomczak, and Max Welling. Attention-based deep multiple instance learning. In *International conference on machine learning*, pp. 2127–2136. PMLR, 2018.

Guillaume Jaume, Paul Doucet, Andrew H. Song, Ming Y. Lu, Cristina Almagro Pérez, Sophia J Wagner, Anurag Jayant Vaidya, Richard J. Chen, Drew FK Williamson, Ahrong Kim, and Faisal Mahmood. HEST-1k: A dataset for spatial transcriptomics and histology image analysis. In *The Thirty-eight Conference on Neural Information Processing Systems Datasets and Benchmarks Track*, 2024a. URL https://openreview.net/forum?id=mlhFJE7PKo.

Guillaume Jaume, Anurag Vaidya, Richard Chen, Drew Williamson, Paul Liang, and Faisal Mahmood. Modeling dense multimodal interactions between biological pathways and histology for survival prediction. *Proceedings of the IEEE/CVF Conference on Computer Vision and Pattern Recognition (CVPR)*, 2024b.

Yuran Jia, Junliang Liu, Li Chen, Tianyi Zhao, and Yadong Wang. Thitogene: a deep learning method for predicting spatial transcriptomics from histological images. *Briefings in Bioinformatics*, 25(1):bbad464, 2024.

Taejong Joo and Uijung Chung. Revisiting explicit regularization in neural networks for reliable predictive probability, 2021. URL https://openreview.net/forum?id=YD792AFzt4o.

Diederik P Kingma. Adam: A method for stochastic optimization. *arXiv preprint arXiv:1412.6980*, 2014.

Vladimir Yu Kiselev, Tallulah S Andrews, and Martin Hemberg. Challenges in unsupervised clustering of single-cell rna-seq data. *Nature Reviews Genetics*, 20(5):273–282, 2019.

Ilya Korsunsky, Nghia Millard, Jean Fan, Kamil Slowikowski, Fan Zhang, Kevin Wei, Yuriy Baglaenko, Michael Brenner, Po-ru Loh, and Soumya Raychaudhuri. Fast, sensitive and accurate integration of single-cell data with harmony. *Nature methods*, 16(12):1289–1296, 2019.

Volodymyr Kuleshov and Percy S Liang. Calibrated structured prediction. *Advances in Neural Information Processing Systems*, 28, 2015.

Jeaung Lee, Jeewoo Lim, Keunho Byeon, and Jin Tae Kwak. Benchmarking pathology foundation models: Adaptation strategies and scenarios. *arXiv preprint arXiv:2410.16038*, 2024a.

Yongju Lee, Xinhao Liu, Minsheng Hao, Tianyu Liu, and Aviv Regev. Pathomclip: Connecting tumor histology with spatial gene expression via locally enhanced contrastive learning of pathology and single-cell foundation model. *bioRxiv*, pp. 2024–12, 2024b.

Zhaoqi Leng, Mingxing Tan, Chenxi Liu, Ekin Dogus Cubuk, Jay Shi, Shuyang Cheng, and Dragomir Anguelov. Polyloss: A polynomial expansion perspective of classification loss functions. In *International Conference on Learning Representations*, 2022. URL https://openreview.net/forum?id=gSdSJoenupI.

Jeremiah Liu, Zi Lin, Shreyas Padhy, Dustin Tran, Tania Bedrax Weiss, and Balaji Lakshminarayanan. Simple and principled uncertainty estimation with deterministic deep learning via distance awareness. *Advances in neural information processing systems*, 33:7498–7512, 2020.

Tianyu Liu, Tinglin Huang, Yingxin Lin, Rex Ying, and Hongyu Zhao. Unicorn: Towards universal cellular expression prediction with an explainable multi-task learning framework. *bioRxiv*, 2025a. doi: 10.1101/2025.01.22.634371. URL https://www.biorxiv.org/content/early/2025/01/25/2025.01.22.634371.

Tianyu Liu, Tinglin Huang, Rex Ying, and Hongyu Zhao. spemo: Exploring the capacity of foundation models for analyzing spatial multi-omic data. *bioRxiv*, pp. 2025–01, 2025b.

Aaron Lou, Chenlin Meng, and Stefano Ermon. Discrete diffusion modeling by estimating the ratios of the data distribution. *arXiv preprint arXiv:2310.16834*, 2023.

Ming Y Lu, Bowen Chen, Drew FK Williamson, Richard J Chen, Ivy Liang, Tong Ding, Guillaume Jaume, Igor Odintsov, Andrew Zhang, Long Phi Le, et al. Towards a visual-language foundation model for computational pathology. *arXiv preprint arXiv:2307.12914*, 2023.

Ming Y Lu, Bowen Chen, Drew FK Williamson, Richard J Chen, Ivy Liang, Tong Ding, Guillaume Jaume, Igor Odintsov, Long Phi Le, Georg Gerber, et al. A visual-language foundation model for computational pathology. *Nature Medicine*, 30(3):863–874, 2024.

Jiabo Ma, Zhengrui Guo, Fengtao Zhou, Yihui Wang, Yingxue Xu, Yu Cai, Zhengjie Zhu, Cheng Jin, Yi Lin, Xinrui Jiang, Anjia Han, Li Liang, Ronald Cheong Kin Chan, Jiguang Wang, Kwang-Ting Cheng, and Hao Chen. Towards a generalizable pathology foundation model via unified knowledge distillation, 2024. URL `https://arxiv.org/abs/2407.18449`.

Prasanta Chandra Mahalanobis. On the generalized distance in statistics. *Sankhyā: The Indian Journal of Statistics, Series A (2008-)*, 80:S1–S7, 2018.

Shie Mannor, Dori Peleg, and Reuven Rubinstein. The cross entropy method for classification. In *Proceedings of the 22nd international conference on Machine learning*, pp. 561–568, 2005.

Leland McInnes, John Healy, Nathaniel Saul, and Lukas Großberger. Umap: Uniform manifold approximation and projection. *Journal of Open Source Software*, 3(29):861, 2018. doi: 10.21105/joss.00861. URL `https://doi.org/10.21105/joss.00861`.

Volodymyr Mnih. Asynchronous methods for deep reinforcement learning. *arXiv preprint arXiv:1602.01783*, 2016.

Jooyoung Moon, Jihyo Kim, Younghak Shin, and Sangheum Hwang. Confidence-aware learning for deep neural networks. In *international conference on machine learning*, pp. 7034–7044. PMLR, 2020.

Jishnu Mukhoti, Viveka Kulharia, Amartya Sanyal, Stuart Golodetz, Philip Torr, and Puneet Dokania. Calibrating deep neural networks using focal loss. *Advances in neural information processing systems*, 33: 15288–15299, 2020.

Rafael Müller, Simon Kornblith, and Geoffrey E Hinton. When does label smoothing help? *Advances in neural information processing systems*, 32, 2019.

Pedro C Neto, Diana Montezuma, Sara P Oliveira, Domingos Oliveira, João Fraga, Ana Monteiro, João Monteiro, Liliana Ribeiro, Sofia Gonçalves, Stefan Reinhard, et al. An interpretable machine learning system for colorectal cancer diagnosis from pathology slides. *NPJ precision oncology*, 8(1):56, 2024.

Muhammad Khalid Khan Niazi, Anil V Parwani, and Metin N Gurcan. Digital pathology and artificial intelligence. *The lancet oncology*, 20(5):e253–e261, 2019.

Mieko Ochi, Daisuke Komura, and Shumpei Ishikawa. Pathology foundation models. *arXiv preprint arXiv:2407.21317*, 2024.

Maxime Oquab, Timothée Darcet, Théo Moutakanni, Huy V. Vo, Marc Szafraniec, Vasil Khalidov, Pierre Fernandez, Daniel HAZIZA, Francisco Massa, Alaaeldin El-Nouby, Mido Assran, Nicolas Ballas, Wojciech Galuba, Russell Howes, Po-Yao Huang, Shang-Wen Li, Ishan Misra, Michael Rabbat, Vasu Sharma, Gabriel Synnaeve, Hu Xu, Herve Jegou, Julien Mairal, Patrick Labatut, Armand Joulin, and Piotr Bojanowski. DINOv2: Learning robust visual features without supervision. *Transactions on Machine Learning Research*, 2024. ISSN 2835-8856. URL `https://openreview.net/forum?id=a68SUt6zFt`. Featured Certification.

Fabian Pedregosa, Gaël Varoquaux, Alexandre Gramfort, Vincent Michel, Bertrand Thirion, Olivier Grisel, Mathieu Blondel, Peter Prettenhofer, Ron Weiss, Vincent Dubourg, et al. Scikit-learn: Machine learning in python. *the Journal of machine Learning research*, 12:2825–2830, 2011.

Gabriel Pereyra, George Tucker, Jan Chorowski, Lukasz Kaiser, and Geoffrey Hinton. Regularizing neural networks by penalizing confident output distributions, 2017. URL `https://openreview.net/forum?id=HkCjNI5ex`.

Silvia L Pintea, Yancong Lin, Jouke Dijkstra, and Jan C van Gemert. A step towards understanding why classification helps regression. In *Proceedings of the IEEE/CVF International Conference on Computer Vision*, pp. 19972–19981, 2023.

Jeffrey M Pullin and Davis J McCarthy. A comparison of marker gene selection methods for single-cell rna sequencing data. *Genome Biology*, 25(1):56, 2024.

Yixuan Qiao, Lianhe Zhao, Chunlong Luo, Yufan Luo, Yang Wu, Shengtong Li, Dechao Bu, and Yi Zhao. Multi-modality artificial intelligence in digital pathology. *Briefings in Bioinformatics*, 23(6):bbac367, 2022.

Muhammad Shaban, Yunhao Bai, Huaying Qiu, Shulin Mao, Jason Yeung, Yao Yu Yeo, Vignesh Shanmugam, Han Chen, Bokai Zhu, Jason L Weirather, et al. Maps: Pathologist-level cell type annotation from tissue images through machine learning. *Nature Communications*, 15(1):28, 2024.

George Shaikovski, Adam Casson, Kristen Severson, Eric Zimmermann, Yi Kan Wang, Jeremy D Kunz, Juan A Retamero, Gerard Oakley, David Klimstra, Christopher Kanan, et al. Prism: A multi-modal generative foundation model for slide-level histopathology. *arXiv preprint arXiv:2405.10254*, 2024.

Jialin Shi, Kailai Zhang, Chenyi Guo, Youquan Yang, Yali Xu, and Ji Wu. A survey of label-noise deep learning for medical image analysis. *Medical image analysis*, 95:103166, 2024.

Andrew H Song, Guillaume Jaume, Drew FK Williamson, Ming Y Lu, Anurag Vaidya, Tiffany R Miller, and Faisal Mahmood. Artificial intelligence for digital and computational pathology. *Nature Reviews Bioengineering*, 1(12):930–949, 2023a.

Dongyuan Song, Kexin Li, Xinzhou Ge, and Jingyi Jessica Li. Clusterde: a post-clustering differential expression (de) method robust to false-positive inflation caused by double dipping. *Research Square*, 2023b.

Hoa Thi Nhu Tran, Kok Siong Ang, Marion Chevrier, Xiaomeng Zhang, Nicole Yee Shin Lee, Michelle Goh, and Jinmiao Chen. A benchmark of batch-effect correction methods for single-cell rna sequencing data. *Genome biology*, 21:1–32, 2020.

Anurag Vaidya, Andrew Zhang, Guillaume Jaume, Andrew H Song, Tong Ding, Sophia J Wagner, Ming Y Lu, Paul Doucet, Harry Robertson, Cristina Almagro-Perez, et al. Molecular-driven foundation model for oncologic pathology. *arXiv preprint arXiv:2501.16652*, 2025.

Shaobo Wang, Yantai Yang, Qilong Wang, Kaixin Li, Linfeng Zhang, and Junchi Yan. Not all samples should be utilized equally: Towards understanding and improving dataset distillation. *arXiv preprint arXiv:2408.12483*, 2024.

Zhou Wang and Alan C Bovik. Mean squared error: Love it or leave it? a new look at signal fidelity measures. *IEEE signal processing magazine*, 26(1):98–117, 2009.

John N Weinstein, Eric A Collisson, Gordon B Mills, Kenna R Shaw, Brad A Ozenberger, Kyle Ellrott, Ilya Shmulevich, Chris Sander, and Joshua M Stuart. The cancer genome atlas pan-cancer analysis project. *Nature genetics*, 45(10):1113–1120, 2013.

F Alexander Wolf, Philipp Angerer, and Fabian J Theis. Scanpy: large-scale single-cell gene expression data analysis. *Genome biology*, 19:1–5, 2018.

Jinxi Xiang and Jun Zhang. Exploring low-rank property in multiple instance learning for whole slide image classification. In *The Eleventh International Conference on Learning Representations*, 2023. URL `https://openreview.net/forum?id=O1KmhBsEPFO`.

Jinxi Xiang, Xiyue Wang, Xiaoming Zhang, Yinghua Xi, Feyisope Eweje, Yijiang Chen, Yuchen Li, Colin Bergstrom, Matthew Gopaulchan, Ted Kim, et al. A vision–language foundation model for precision oncology. *Nature*, pp. 1–10, 2025.

Ronald Xie, Kuan Pang, Sai Chung, Catia Perciani, Sonya MacParland, Bo Wang, and Gary Bader. Spatially resolved gene expression prediction from histology images via bi-modal contrastive learning. *Advances in Neural Information Processing Systems*, 36, 2024.

Hanwen Xu, Naoto Usuyama, Jaspreet Bagga, Sheng Zhang, Rajesh Rao, Tristan Naumann, Cliff Wong, Zelalem Gero, Javier González, Yu Gu, et al. A whole-slide foundation model for digital pathology from real-world data. *Nature*, pp. 1–8, 2024a.

Yingxue Xu, Yihui Wang, Fengtao Zhou, Jiabo Ma, Shu Yang, Huangjing Lin, Xin Wang, Jiguang Wang, Li Liang, Anjia Han, et al. A multimodal knowledge-enhanced whole-slide pathology foundation model. *arXiv preprint arXiv:2407.15362*, 2024b.

Yuansong Zeng, Zhuoyi Wei, Weijiang Yu, Rui Yin, Yuchen Yuan, Bingling Li, Zhonghui Tang, Yutong Lu, and Yuedong Yang. Spatial transcriptomics prediction from histology jointly through transformer and graph neural networks. *Briefings in Bioinformatics*, 23(5):bbac297, 2022.

Andrew Zhang, Guillaume Jaume, Anurag Vaidya, Tong Ding, and Faisal Mahmood. Accelerating data processing and benchmarking of ai models for pathology. *arXiv preprint arXiv:2502.06750*, 2025.

Jingfeng Zhang, Bo Song, Haohan Wang, Bo Han, Tongliang Liu, Lei Liu, and Masashi Sugiyama. Badlabel: A robust perspective on evaluating and enhancing label-noise learning. *IEEE transactions on pattern analysis and machine intelligence*, 46(6):4398–4409, 2024.

Shaoting Zhang and Dimitris Metaxas. On the challenges and perspectives of foundation models for medical image analysis. *Medical image analysis*, 91:102996, 2024.

Shihao Zhang, Linlin Yang, Michael Bi Mi, Xiaoxu Zheng, and Angela Yao. Improving deep regression with ordinal entropy. In *The Eleventh International Conference on Learning Representations*, 2023. URL `https://openreview.net/forum?id=raUO7GpPOP`.

Sichen Zhu, Yuchen Zhu, Molei Tao, and Peng Qiu. Diffusion generative modeling for spatially resolved gene expression inference from histology images. In *The Thirteenth International Conference on Learning Representations*, 2025. URL `https://openreview.net/forum?id=FtjLUHyZAO`.

Weiyao Zhu, Ou Wu, Fengguang Su, and Yingjun Deng. Exploring the learning difficulty of data: Theory and measure. *ACM Transactions on Knowledge Discovery from Data*, 18(4):1–37, 2024.

6 Appendix

In this section, we present information on baselines, hyper-parameters, and other analyses or tables that cannot be placed in the main text due to page limitation.

6.1 Visualization of Sample Difficulty.

Here we visualize the sample label as well as sample difficulty based on the TCGA dataset with UNI v1 embeddings Figure 6 based on UMAP McInnes et al. (2018). According to this figure, we capture sample difficulty of different labels, and the samples with similar difficulty levels show clustering performances. This discovery further conforms our interpretation of sample difficulty.

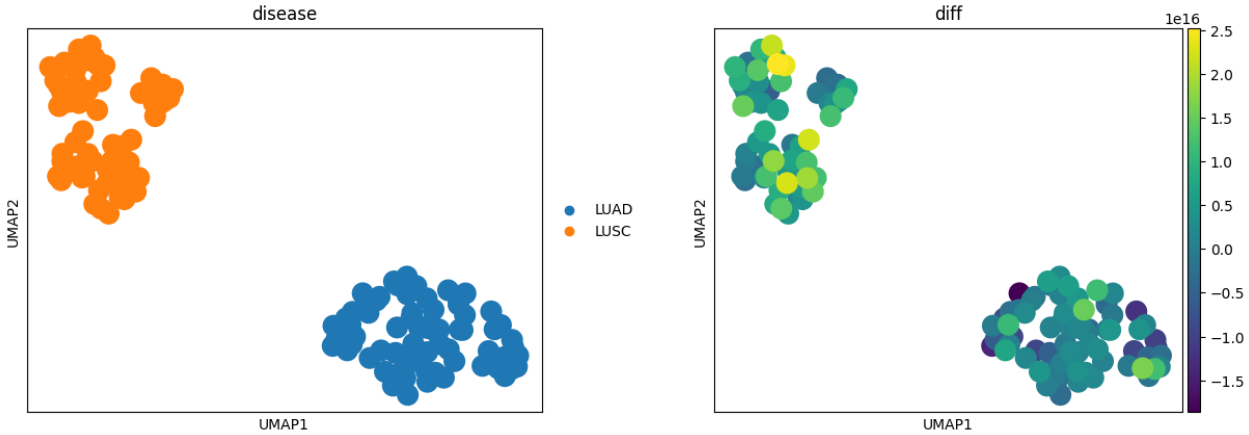

Figure 6: UMAP visualization of sample embeddings colored by disease states (left) and sample difficulty (right).

6.2 Motivations and Stability of *MRMD*.

Motivation explanation.

According to Figure 7, we found that Logistic Regression (LR) can make correct prediction for samples with high difficulty levels, as well as wrong prediction for samples with low difficulty levels. This observation motivates us to reconsider the design of sample difficulty estimation, as we need to include the prior from a simple regression before estimating the sample difficulty with a more complicated model. Since the main purpose of considering sample difficulty is to improve generalizability by correctly predicting difficult samples, we believe it is necessary to reconsider the definition of difficult samples.

Stability explanation.

We ensure the stability of sample difficulty estimation by examining the consistency of the proportion of wrongly classified labels with different numbers of cross-validation sets. Our assumption is that the adjustment of cross-validation numbers will not affect the proportion of such samples. Here we show the proportion overlap by iterating different split q in Tables 3 and 4, and we do not observe strong oscillation by iterating different q for the three datasets used in the classification task. Therefore, our proposed method can define a robust method for generating difficult samples.

Number of split	2	3	4	5	6	7	8	9	10
Proportion	0.46	0.43	0.49	0.49	0.47	0.44	0.44	0.43	0.43

Table 3: Relationship between the number of splits and the proportion of difficult samples identified by LR model in the CAMELYON16 dataset.

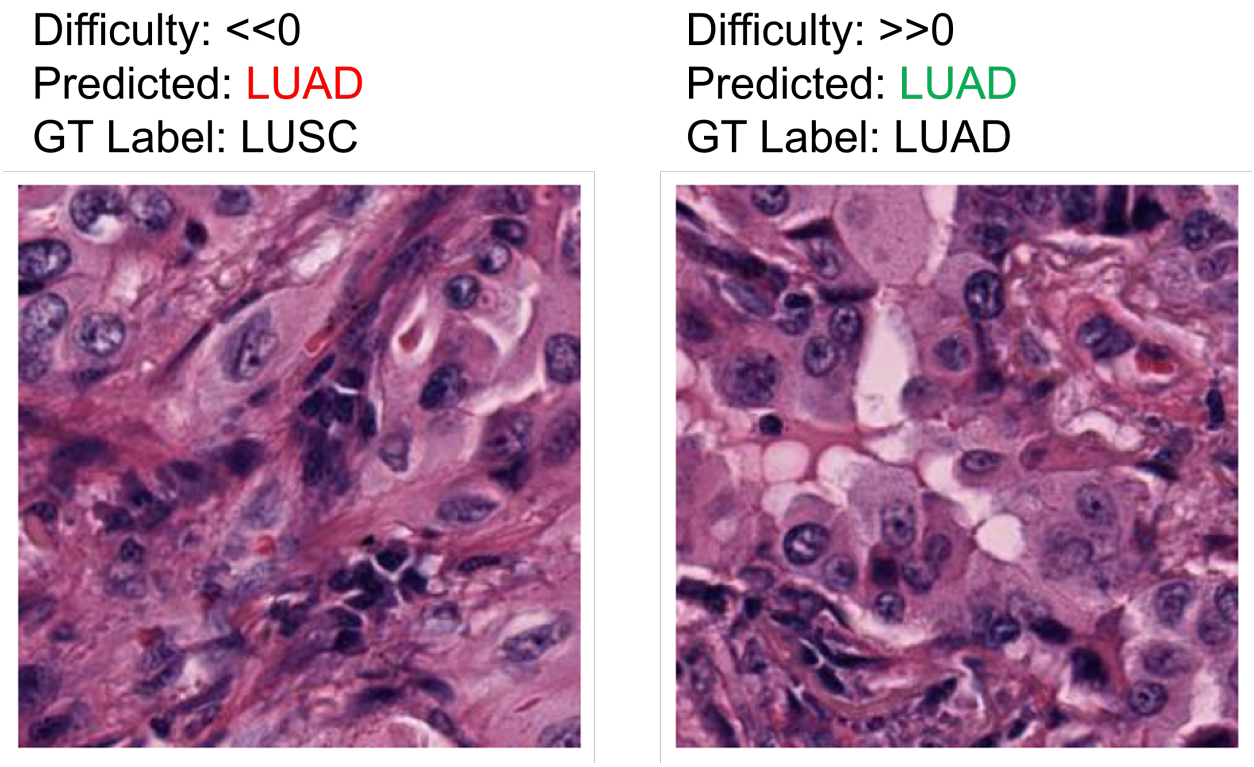

Figure 7: Examples of histopathology images and corresponding decisions made by LR, which is based on ResNet 50 and TCGA dataset.

Number of split	2	3	4	5	6	7	8	9	10
Proportion	0.59	0.57	0.56	0.56	0.55	0.56	0.55	0.55	0.55

Table 4: Relationship between the number of splits and the proportion of difficult samples identified by LR model in the PANDA dataset.

We also accumulate the proportion of samples with lowest sample difficulty after min-max normalization across three datasets in Table 5.

Dataset	**Proportion**
TCGA	0.76 %
CAMELYON16	0.66 %
PANDA	0.009 %

Table 5: Label proportion.

6.3 Comparison between RMD and USD.

- Different scenarios: Cui et al. (2023) focuses on a general computer vision problem with public datasets from different domains, but USD aims to tackle a challenge mentioned in the potential limitations of Cui et al. (2023), which focuses on medical image analysis, as the medical images suffer from more challenging scenarios, such as label imbalance and noisy data. Cui et al. (2023) is not straightforwardly suitable for medical domain data.
- Different problem settings: In terms of problem construction, Cui et al. (2023) only considers image classification as a major task, while USD considers more diverse tasks, including image classification

as well as gene expression prediction (a regression task). We are among the first research groups that try to improve the image regression prediction performance by leveraging the estimated sample difficulty, and thus USD is a more generalizable tool. Moreover, extending the estimation method to regression problems is not easily shown in our comprehensive experiments and discussion.

- Different difficult estimation methods: In terms of the estimation of sample difficulty, Cui et al. (2023) does not consider any prior information which might help on the estimation process, while USD considers using a simpler classifier such as Logistic Regression to provide correct prior to estimate a more accurate sample difficulty, supported by the visualization result in Figure 1 and the performance improvement across different tasks.

- Different experimental designs: Cui et al. (2023) did not consider many ablation studies and did not justify the necessity of introducing sample difficulty estimation for different datasets, as it lacked comparison with a linear-based classifier, but USD introduces a more rigorous comparison and demonstrates that we need to figure out the complexity of the problem ahead of model training and construction. USD also has more ablation studies to justify our choices for both the classification and regression tasks. Therefore, USD improves significantly and generalizes to a different area compared with Cui et al. (2023), which leads to an independent method.

6.4 Label Distribution of Imbalance and Noisy Data Testing.

Label distributions of datasets designed for the classification task.

Type	TCGA_number
tumor	100
health	90

Table 6: Label distribution of the TCGA dataset.

Type	CAMELYON16_number
tumor	159
health	111

Table 7: Label distribution of the CAMELYON16 dataset.

Index	PANDA_number
0	2892
1	2666
2	1343
4	1249
3	1242
5	1224

Table 8: Label distribution of the PANDA dataset.

Analysis of label imbalance testing.

To produce data with imbalanced labels, we now include more experiment results based on sampling the labels to create an extreme imbalance dataset from CAMELYON16, shown in Table 9, including the case of many positive samples and the case of many negative samples. According to the results from this table, USD still performs well under the extreme conditions, achieving over 80% accuracy under two situations. Compared with the original dataset, we even have better performance, and thus USD will not be affected by the issue of label imbalance significantly.

Analysis of label noise testing.

Dataset	Model	Metric	Original	Many positive samples (pos/neg=7)	Many negative samples (neg/pos=14)
CAMELYON16	UNI v1+USD (Poly)	ACC	0.756 (0.02)	0.850 (0.03)	0.949 (0.01)
		wF1	0.746 (0.03)	0.804 (0.01)	0.804 (0.01)
	UNI v1+USD (ER)	ACC	0.741 (0.03)	0.831 (0.03)	0.977 (0.00)
		wF1	0.750 (0.03)	0.988 (0.00)	0.766 (0.01)

Table 9: Performances of USD with two different sample difficulty penalty methods under three conditions with label imbalance simulation.

To produce data with noisy labels, we utilize the symmetric noise generation method used in trustworthy machine learning Zhang et al. (2024) and discrete diffusion models Lou et al. (2023), which means we select a certain proportion of samples and randomly pick different labels to replace their correct labels. We then train USD with pathology image features from UNI v1 for the classification task. According to Table 10 with Accuracy, AUROC, and wF1 metrics, we find that USD still shows good performances under the condition with relatively lower noise label proportion (0.1-0.3), and the performance USD will be affected under high noise level proportion, which aligns with the study of label noise shown in Zhang et al. (2024). Therefore, USD is still a robust mode for datasets with a small amount of imperfect labels. In real applications, for datasets with a very high proportion of imperfect labels, which might be caused by low data quality and the calibration with domain experts, label re-annotation, loss re-design could be more suitable approaches in medical applications Shi et al. (2024).

Dataset	Metric	0.1	0.3	0.5	0.7
TCGA	ACC	0.910 (0.05)	0.923 (0.05)	0.920 (0.03)	0.090 (0.04)
	AUROC	0.991 (0.01)	0.992 (0.01)	0.990 (0.01)	0.016 (0.02)
CAMELYON16	ACC	0.665 (0.02)	0.594 (0.04)	0.526 (0.04)	0.365 (0.04)
	AUROC	0.798 (0.02)	0.671 (0.01)	0.491 (0.04)	0.319 (0.03)
PANDA	ACC	0.461 (0.01)	0.429 (0.00)	0.389 (0.01)	0.295 (0.04)
	wF1	0.438 (0.01)	0.396 (0.01)	0.340 (0.03)	0.217 (0.07)

Table 10: Model performances with the format score (standard deviation) under different noise levels (0.1–0.7) for the classification task.

We have also designed experiments to test the relationship between poisoned labels and MRMD difficulty. Based on the embeddings from the model UNI and the dataset CAMELYON16, we considered flipping three different proportions of labels to introduce label noise (0.05, 0.1, and 0.20), and compared the MRMD between samples with cleaned labels and samples with noisy labels. According to Table **??**, we observed a large difficulty value under all three conditions, supported by the positive Mean Poison-Clean MRMD Delta score. Moreover, we computed both the Paired $t-$test p-value and the Wilcoxon Rank-sum test p-value, and the results showed that the difference is also significant. Therefore, our difficulty estimation method can clearly reflect the difference between samples that are easier to predict and those that are more difficult to predict, and thus it can better assist prediction-related tasks.

Flip Rate	Mean Poison-Clean MRMD Delta	Paired t-test p	Wilcoxon p
0.05	4.254	0.0257	0.0375
0.10	4.429	0.00243	0.00106
0.20	5.247	1.97×10^{-7}	4.95×10^{-7}

Table 11: Statistical comparison of MRMD changes across flip rates.

6.5 Explanations of Baselines

Explanations of Baseline Methods for Disease-State Classification.

Let p_k be the likelihood that the model assigned to the k-th class given the input $\mathbf{x}$, and y_k is the true target, where y_k is 1 for the correct class and 0 for the rest.

- Cross Entropy (CE): $\mathcal{L}_{\text{CE}} = -\sum_{k=1}^{K} y_k \log p_k$.
- Label Smoothing (LS): $\mathcal{L}_{\text{LS}} = -\sum_{k=1}^{K} y_k^{\text{LS}} \log p_k$ with $y_k^{\text{LS}} = y_k(1-\alpha) + \alpha/K$ and α is a tuning parameter.
- Focal Loss: $\mathcal{L}_{\text{Focal}} = -\sum_{k=1}^{K} y_k(1-p_k)^{\gamma} \log p_k$, where γ is a tuning parameter.
- Entropy Regularizer (ER): $\mathcal{L}_{\text{ER}} = \mathcal{L}_{\text{CE}} - \alpha\mathcal{H}(p)$, where $\mathcal{H}(p) = -\sum_{k=1}^{K} p_k \log p_k$ and α is a tuning parameter.
- Poly-N Loss: $\mathcal{L}_{\text{Poly}} = \mathcal{L}_{\text{CE}} + \sum_{k=1}^{K} y_k \sum_{j=1}^{N} \epsilon_j (1-p_k)^j$ where ϵ_j is the perturbation term for the j-th coefficient.
- L_1 Loss: $\mathcal{L}_{L_1} = \mathcal{L}_{\text{CE}} + \lambda \|f_W\|_1$ where $f_W \in \mathbb{R}^K$ is the logit values, and we use it to compute $p_k = \text{softmax}_k(f_W)$.
- Weighted ER: $\mathcal{L}_{\text{WER}} = \mathcal{L}_{\text{CE}} - \alpha s(\mathbf{x}, y)\mathcal{H}(p)$, where α is a tuning parameter and $s(\mathbf{x}, y)$ is a sample-specific weighting derived from the RMD-based sample difficulty score.
- Weighted Poly-1:
$$\mathcal{L}_{\text{WPoly}} = \mathcal{L}_{\text{CE}} + s(\mathbf{x}, y) \sum_{k=1}^{K} y_k \epsilon_1 (1-p_k),$$
where $s(\mathbf{x}, y)$ is a sample-specific weighting derived from the RMD-based sample difficulty score.

Explanations of Baseline Methods for Gene Expression Prediction.

Let y be the true target and $f(\mathbf{x})$ be the prediction based on the input $\mathbf{x}$.

- MSE Loss: $\mathcal{L}_{\text{MSE}} = (y - f(\mathbf{x}))^2$.
- Huber Loss: Given a hyper-parameter δ,
$$\mathcal{L}_{\text{Huber}} = \begin{cases} \frac{1}{2}(y - f(\mathbf{x}))^2 & \text{if } |y - f(\mathbf{x})| \leq \delta \\ \delta(|y - f(\mathbf{x})| - \frac{1}{2}\delta) & \text{otheriwse} \end{cases}.$$

Explanations of Methods for Reducing Batch Effect. Batch effect means the technique noise existing in the sequencing data from different samples. We consider Harmony Korsunsky et al. (2019) and KBins Pedregosa et al. (2011) as two approaches for reducing batch effect. The idea of Harmony is to utilize iterative clustering to pull the cells (spots) from different samples with similar biological information to a cluster, until the convergence. This approach has been validated by several benchmarking studies Tran et al. (2020); Arevalo et al. (2024) as a suitable method. KBins means we utilize k-bin discreter to place spots with similar average gene expression profiles across genes in a cluster, and thus the batch effect can be reduced by better characterizing biology-informed clusters.

6.6 Hyper-parameter Tuning

For the disease-state classification task, we inherit the loss-specific hyper-parameter from Cui et al. (2023), which is already tuned. These parameters include the entropy weight $\lambda_e = 0.3$, the Focal weight $f_\gamma = 1.0$, the LS weight $\epsilon = 1.0$, the L_1 weight $\alpha = 1.0$, and the Poly weight $\epsilon_p = 2.0$. The learning rate for training different combinations with PANDA and CAMELYON16 is 1e-3. The learning rate for training different combinations based on UNI v1, UNI v2, and GigaPath is 1e-3, and 1e-2 based on ResNet 50, for the TCGA dataset. The choice of fold s is explained in the Analysis section. In this section, we present information on baselines, hyper-parameters, and other analyses or tables that cannot be placed in the main text due to page limitations.

For the gene expression prediction task, we tune the learning rate, λ_{OE}, and λ_f based on the grid search for all models. The final choices of these three parameters are summarized in Table 12. We found that the change of these choices is not in a large range, and thus our model is robust for different conditions. The choice of fold s is explained in the Analysis section.

Dataset	Learning Rate	λ_{OE}	λ_f
IDC	1.00E-04	1.00E-03	1.00E-03
READ	1.00E-03	1.00E-03	1.00E-03
PRAD	1.00E-03	1.00E-03	1.00E-03
LYMPH_IDC	1.00E-03	1.00E-03	1.00E-02
COAD	1.00E-03	1.00E-03	1.00E-03
CCRCC	1.00E-03	1.00E-03	1.00E-03
Brain	1.00E-03	1.00E-03	1.00E-03
Skin	1.00E-03	1.00E-03	1.00E-03

Table 12: Hyper-parameter tuning information of the spatial transcriptomic prediction task.

6.7 Training Efficiency

Here we present the running time and consumed GPU memory in Table 13 for the classification task and Table 14 for the regression task. According to these tables, USD consumes comparable resources with other baselines, but can improve model performances.

Method	Time (s)	GPU memory usage (GB)
LS	68.457	4.725
L_1	73.973	4.725
Focal	60.086	4.725
Poly	68.852	4.725
ER	77.329	4.266
CE	79.456	4.725
WER	111.930	4.396
Wpoly	108.710	4.396
USD (Poly)	108.710	4.396

Table 13: Running time and memory usage for the classification task. We include statistics from both baseline methods and USD. The experiment is performed on the CAMELYON16 dataset.

Method	Time (s)	GPU memory usage (GB)
MSE Loss	307.252	5.930
Huber Loss	306.928	5.930
PCCMSE Loss	335.070	5.930
USD (ER)	931.392	11.129

Table 14: Running time and memory usage for the classification task. We include statistics from both baseline methods and USD. The experiment is performed on the Brain dataset.

6.8 Full Tables

We list the average scores of all metrics for the classification task in Table 15, the standard deviation of all metrics for the classification task in Table 16, and the standard deviation of all metrics for the regression task in Table 17.

Datasets	Metrics	Base	Methods										
			LS	L_1	Focal	Poly	ER	CE	WER	WPoly	**USD (ER)**	**USD (Poly)**	Best Method
TCGA	ACC (↑)	UNI v1	0.420	0.923	0.913	0.927	**0.933**	0.913	**0.933**	0.923	**0.933**	0.923	UNI v2+USD (ER)
		UNI v2	0.520	0.960	0.933	0.930	0.963	0.923	**1.000**	0.920	**1.000**	0.920	
		GigaPath	0.510	0.647	0.603	0.760	0.697	0.737	0.677	**0.767**	0.677	**0.767**	
		ResNet 50	0.517	0.517	0.653	0.637	0.520	0.643	0.640	**0.690**	0.627	0.680	
	AUROC (↑)	UNI v1	0.446	0.986	0.987	0.986	**0.994**	0.986	0.994	0.989	**0.994**	0.989	UNI v2+USD (ER)
		UNI v2	0.543	**1.000**	**1.000**	**1.000**	0.997	**1.000**	**1.000**	**1.000**	**1.000**	**1.000**	
		GigaPath	0.570	0.742	0.838	0.859	0.877	0.866	**0.898**	0.891	**0.898**	0.891	
		ResNet 50	0.545	0.517	0.704	0.697	0.568	0.696	0.664	0.721	0.677	**0.731**	
	Bacc (↑)	UNI v1	0.420	0.923	0.913	0.927	**0.933**	0.913	**0.933**	0.923	**0.933**	0.923	UNI v2+USD (ER)
		UNI v2	0.520	0.960	0.933	0.930	0.963	0.923	**1.000**	0.920	**1.000**	0.920	
		GigaPath	0.510	0.647	0.603	0.760	0.697	0.737	0.677	**0.767**	0.677	**0.767**	
		ResNet 50	0.517	0.517	0.653	0.637	0.520	0.643	0.640	**0.690**	0.627	0.680	
	Kappa (↑)	UNI v1	-0.160	0.847	0.827	0.853	**0.867**	0.827	0.867	**0.847**	**0.867**	0.847	UNI v2+USD (ER)
		UNI v2	0.040	0.920	0.867	0.860	0.927	0.847	**1.000**	0.840	**1.000**	0.840	
		GigaPath	0.020	0.293	0.207	0.520	0.393	0.473	0.353	**0.533**	0.353	**0.533**	
		ResNet 50	0.033	0.033	0.307	0.273	0.040	0.287	0.280	**0.380**	0.253	0.360	
	wF1 (↑)	UNI v1	0.361	0.923	0.913	0.926	**0.933**	0.913	**0.933**	0.923	**0.933**	0.923	UNI v2+USD (ER)
		UNI v2	0.467	0.960	0.933	0.930	0.963	0.923	**1.000**	0.919	**1.000**	0.919	
		GigaPath	0.447	0.636	0.532	0.749	0.639	0.721	0.627	**0.758**	0.627	**0.758**	
		ResNet 50	0.488	0.442	0.651	0.631	0.438	0.636	0.629	**0.690**	0.613	0.676	
	ECE (↓)	UNI v1	0.107	0.242	0.100	0.089	**0.051**	0.098	0.065	0.097	0.065	0.097	UNI v1+ER
		UNI v2	0.186	0.299	0.073	**0.069**	0.243	0.078	0.151	0.073	0.151	0.073	
		GigaPath	0.131	0.166	0.253	**0.121**	0.227	0.137	0.208	0.126	0.208	0.126	
		ResNet 50	0.210	0.199	**0.155**	0.210	0.219	0.219	0.184	0.209	0.184	0.209	
CAMELYON16	ACC (↑)	UNI v1	0.494	0.715	0.715	0.726	0.732	0.747	0.724	0.724	0.741	**0.756**	UNI v1+USD (Poly)
		UNI v2	0.450	0.574	**0.585**	0.559	0.553	0.559	0.538	0.518	0.562	0.550	
		GigaPath	0.491	0.491	0.468	0.459	0.482	**0.497**	0.488	0.462	0.491	0.485	
		ResNet 50	0.541	0.535	0.529	0.524	0.497	0.521	0.456	0.535	**0.585**	0.553	
	AUROC (↑)	UNI v1	0.536	0.828	0.821	0.832	0.831	0.829	0.821	0.820	0.812	**0.834**	UNI v1+USD (Poly)
		UNI v2	0.463	0.752	0.690	0.738	0.738	0.724	0.701	0.713	**0.753**	0.739	
		GigaPath	0.519	**0.649**	0.593	0.619	0.610	0.610	0.592	0.575	0.643	0.661	
		ResNet 50	0.524	0.725	0.720	0.719	0.719	0.725	0.515	0.712	**0.730**	0.703	
	Bacc (↑)	UNI v1	0.491	0.734	0.733	0.746	0.752	0.765	0.741	0.738	0.757	**0.771**	UNI v1+USD (WPoly)
		UNI v2	0.456	0.605	0.615	0.592	0.587	**0.593**	0.573	0.553	0.592	0.586	
		GigaPath	0.516	0.527	0.510	0.503	0.515	**0.536**	0.525	0.505	0.531	0.526	
		ResNet 50	0.539	0.571	0.565	0.562	0.536	0.558	0.500	0.572	**0.617**	0.588	
	Kappa (↑)	UNI v1	-0.017	0.449	0.448	0.472	0.484	0.510	0.463	0.460	0.496	**0.525**	UNI v1+USD (WPoly)
		UNI v2	-0.087	0.197	**0.218**	0.173	0.163	0.174	0.137	0.100	0.173	0.160	
		GigaPath	0.030	0.050	0.018	0.005	0.029	**0.067**	0.047	0.010	0.060	0.049	
		ResNet 50	0.077	0.133	0.122	0.114	0.068	0.108	0.000	0.135	**0.219**	0.165	
	wF1 (↑)	UNI v1	0.494	0.702	0.704	0.715	0.721	0.739	0.715	0.718	**0.750**	0.746	UNI v1+USD (ER)
		UNI v2	0.435	0.510	**0.521**	0.482	0.475	0.479	0.445	0.407	0.498	0.463	
		GigaPath	**0.413**	0.385	0.316	0.292	0.378	0.378	0.366	0.298	0.350	0.342	
		ResNet 50	**0.534**	0.446	0.438	0.417	0.371	0.417	0.286	0.438	0.524	0.467	
	ECE (↓)	UNI v1	**0.066**	0.102	0.100	0.139	0.092	0.110	0.080	0.133	0.107	0.106	ResNet 50+LS
		UNI v2	**0.058**	0.114	0.103	0.199	0.119	0.144	0.135	0.229	0.159	0.156	
		GigaPath	**0.070**	0.142	0.163	0.342	0.164	0.194	0.188	0.324	0.199	0.232	
		ResNet 50	**0.049**	0.100	0.106	0.245	0.137	0.181	0.190	0.193	0.137	0.167	
PANDA	ACC (↑)	UNI v1	0.147	0.489	0.484	0.490	0.474	0.471	0.485	0.485	**0.495**	0.494	UNI v1+USD (ER)
		UNI v2	0.165	0.479	0.479	**0.489**	0.480	0.479	0.474	0.485	0.488	0.468	
		GigaPath	0.182	0.468	0.459	0.470	0.460	0.465	0.460	0.466	**0.473**	0.453	
		ResNet 50	0.178	0.417	0.437	0.440	0.437	**0.439**	0.429	0.438	0.430	0.431	
	wF1 (↑)	UNI v1	0.099	0.458	0.468	0.467	0.445	0.446	0.467	0.469	**0.479**	0.478	UNI v1+USD (ER)
		UNI v2	0.165	0.479	0.479	**0.489**	0.480	0.479	0.474	0.485	0.488	0.468	
		GigaPath	0.171	0.437	0.435	0.445	0.438	0.446	0.428	0.440	**0.455**	0.424	
		ResNet 50	0.174	0.342	**0.416**	0.413	0.415	**0.416**	0.403	0.413	0.397	0.404	
	Bacc (↑)	UNI v1	0.162	0.422	0.432	0.431	0.413	0.411	0.432	0.431	**0.437**	0.441	UNI v1+USD (ER)
		UNI v2	0.170	0.408	0.426	0.431	0.423	0.425	0.417	**0.433**	0.428	0.405	
		GigaPath	0.161	0.398	0.398	0.410	0.399	0.408	0.392	0.399	**0.414**	0.388	
		ResNet 50	0.179	0.333	0.377	**0.381**	0.378	0.379	0.366	0.380	0.368	0.368	
	Kappa (↑)	UNI v1	0.002	0.589	0.605	0.598	0.588	0.582	0.598	**0.599**	0.594	0.603	UNI v2+Focal
		UNI v2	0.004	0.588	**0.613**	0.602	0.611	0.604	0.605	0.612	0.603	0.585	
		GigaPath	0.000	0.568	0.574	**0.590**	0.576	0.582	0.564	0.570	0.577	0.567	
		ResNet 50	0.048	0.476	0.524	**0.533**	0.524	0.531	0.518	0.530	0.527	0.517	
	ECE (↓)	UNI v1	0.047	0.088	**0.023**	0.150	0.059	0.045	0.027	0.103	0.043	0.084	ResNet 50+LS
		UNI v2	0.033	0.101	**0.032**	0.128	0.067	0.045	0.041	0.077	0.034	0.051	
		GigaPath	**0.016**	0.086	0.027	0.150	0.064	0.054	0.043	0.074	0.031	0.061	
		ResNet 50	**0.012**	0.099	0.050	0.096	0.082	0.018	0.056	0.057	0.022	0.022	

Table 15: Benchmarking average scores under the full metric list for the classification task.

Datasets	Metrics	Base	Methods										
			LS	L_1	Focal	Poly	ER	CE	WER	WPoly	**USD (ER)**	**USD (Poly)**	Best Method
TCGA	ACC	UNI v1	0.072	0.028	0.022	0.009	**0.000**	0.022	**0.000**	0.015	**0.000**	0.015	UNI v2+USD (ER)
		UNI v2	0.230	0.022	0.017	0.014	0.022	0.015	**0.000**	0.007	**0.000**	0.007	
		GigaPath	0.162	0.151	0.076	0.067	0.180	0.069	0.134	**0.024**	0.134	**0.024**	
		ResNet 50	0.249	0.054	0.032	0.043	0.051	0.032	0.043	**0.022**	0.035	0.046	
	AUROC	UNI v1	0.149	0.010	0.010	0.009	0.008	0.012	**0.005**	0.009	**0.005**	0.009	UNI v2+USD (ER)
		UNI v2	0.264	**0.001**	**0.000**	**0.000**	0.005	**0.000**	**0.000**	**0.000**	**0.000**	**0.000**	
		GigaPath	0.457	0.218	0.071	0.057	0.085	**0.029**	0.047	0.044	0.047	0.044	
		ResNet 50	0.320	0.061	0.024	0.019	0.022	0.016	0.014	**0.012**	0.027	0.032	
	Bacc	UNI v1	0.072	0.028	0.022	0.009	**0.000**	0.022	**0.000**	0.015	**0.000**	0.015	UNI v2+USD (ER)
		UNI v2	0.230	0.022	0.017	0.014	0.022	0.015	**0.000**	0.007	**0.000**	0.007	
		GigaPath	0.162	0.151	0.076	0.067	0.180	0.069	0.134	**0.024**	0.134	**0.024**	
		ResNet 50	0.249	0.054	0.032	0.043	0.051	0.032	0.043	**0.022**	0.035	0.046	
	Kappa	UNI v1	0.144	0.056	0.043	0.018	**0.000**	0.043	**0.000**	0.030	**0.000**	0.030	UNI v2+USD (ER)
		UNI v2	0.460	0.045	0.033	0.028	0.043	0.030	**0.000**	0.015	**0.000**	0.015	
		GigaPath	0.324	0.302	0.152	0.135	0.361	0.138	0.267	**0.047**	0.267	**0.047**	
		ResNet 50	0.499	0.108	0.064	0.086	0.101	0.065	0.087	**0.045**	0.069	0.092	
	wF1	UNI v1	0.074	0.028	0.022	0.009	**0.000**	0.022	**0.000**	0.015	**0.000**	0.015	UNI v2+USD (ER)
		UNI v2	0.250	0.022	0.017	0.014	0.022	0.015	**0.000**	0.008	**0.000**	0.008	
		GigaPath	0.175	0.154	0.128	0.080	0.244	0.086	0.169	**0.027**	0.169	**0.027**	
		ResNet 50	0.272	0.101	0.034	0.045	0.090	0.038	0.067	**0.023**	0.047	0.048	
	ECE	UNI v1	0.057	0.016	0.027	0.013	0.012	0.024	0.024	**0.011**	0.024	**0.011**	UNI v2+Wpoly
		UNI v2	0.103	0.024	0.011	0.011	0.029	0.017	0.050	**0.010**	0.050	**0.010**	
		GigaPath	0.071	0.109	0.089	0.040	0.098	0.072	0.066	**0.014**	0.066	**0.014**	
		ResNet 50	0.085	0.034	0.023	0.035	0.064	0.026	**0.019**	0.029	0.029	0.040	
CAMELYON16	ACC	UNI v1	0.087	0.046	0.040	0.035	0.019	0.019	0.019	0.012	0.034	**0.022**	UNI v1+USD (Poly)
		UNI v2	0.066	0.044	**0.081**	0.063	0.042	0.071	0.069	0.092	0.061	0.054	
		GigaPath	0.095	0.045	0.026	0.007	0.026	**0.035**	0.043	0.013	0.079	0.066	
		ResNet 50	0.039	0.034	0.037	0.049	0.056	0.056	0.000	0.049	**0.056**	0.064	
	AUROC	UNI v1	0.112	0.026	0.047	0.019	0.025	0.026	0.013	0.024	0.026	**0.020**	ResNet 50+Focal
		UNI v2	0.100	0.042	0.091	0.058	0.026	0.040	0.057	0.051	**0.048**	0.039	
		GigaPath	0.097	**0.076**	0.063	0.035	0.096	0.068	0.062	0.052	0.089	0.055	
		ResNet 50	0.089	0.008	**0.002**	0.009	0.011	0.009	0.072	0.015	0.003	0.021	
	Bacc	UNI v1	0.088	0.042	0.036	0.033	0.016	0.017	0.020	**0.015**	0.037	0.019	ResNet 50+ER
		UNI v2	0.072	**0.037**	0.071	0.056	**0.037**	0.063	0.061	0.081	0.052	0.049	
		GigaPath	0.091	0.044	0.022	0.006	0.022	0.032	0.031	**0.012**	0.070	0.058	
		ResNet 50	0.043	0.030	0.032	0.045	0.049	0.050	**0.000**	0.044	0.051	0.058	
	Kappa	UNI v1	0.174	0.083	0.072	0.065	0.034	0.035	0.038	**0.027**	0.069	0.040	ResNet 50+ER
		UNI v2	0.141	0.071	0.137	0.105	**0.070**	0.119	0.115	0.154	0.099	0.092	
		GigaPath	0.179	0.081	0.041	**0.011**	0.040	0.059	0.060	0.022	0.133	0.110	
		ResNet 50	0.043	0.032	0.062	0.084	0.093	0.050	**0.000**	0.044	0.051	0.058	
	wF1	UNI v1	0.087	0.058	0.049	0.041	0.024	0.023	0.020	**0.011**	0.032	0.027	ResNet 50+ER
		UNI v2	**0.067**	0.082	0.144	0.121	0.082	0.129	0.131	0.171	0.122	0.095	
		GigaPath	0.149	0.092	0.067	**0.014**	0.092	0.071	0.111	0.028	0.143	0.126	
		ResNet 50	0.036	0.066	0.072	0.095	0.113	0.102	**0.000**	0.085	0.100	0.116	
	ECE	UNI v1	0.049	0.011	0.026	0.033	**0.006**	0.018	0.021	0.010	0.017	0.019	UNI v1+ER
		UNI v2	0.061	**0.022**	0.038	0.066	0.036	0.054	0.047	0.062	0.043	**0.022**	
		GigaPath	0.055	0.046	0.043	0.051	**0.039**	0.083	0.080	**0.039**	0.043	0.060	
		ResNet 50	0.026	0.037	**0.009**	0.044	0.059	0.017	0.025	0.014	0.047	0.046	
PANDA	ACC	UNI v1	0.050	0.016	0.015	0.016	0.013	0.008	0.011	0.012	**0.014**	0.009	UNI v1+USD (ER)
		UNI v2	0.041	0.011	0.007	**0.005**	0.007	0.004	0.009	0.015	0.010	0.009	
		GigaPath	0.014	0.009	0.012	0.013	0.017	0.003	0.009	0.006	**0.006**	0.007	
		ResNet 50	0.013	0.009	0.005	0.007	0.009	**0.009**	0.005	0.005	0.012	0.012	
	wF1	UNI v1	0.059	0.024	0.019	0.026	0.021	0.014	0.019	0.019	**0.014**	0.010	UNI v1+USD (ER)
		UNI v2	0.047	0.023	0.017	**0.014**	0.015	0.011	0.016	0.021	0.015	0.016	
		GigaPath	0.010	0.016	0.015	0.020	0.025	0.010	0.013	0.006	**0.010**	0.006	
		ResNet 50	0.018	0.018	**0.007**	0.011	0.012	**0.008**	0.011	0.011	0.021	0.026	
	Bacc	UNI v1	0.012	0.021	0.013	0.023	0.016	0.013	0.017	0.017	0.016	**0.008**	GigaPath+Wpoly
		UNI v2	**0.006**	0.015	0.008	0.014	0.011	0.010	0.013	0.012	0.015	0.009	
		GigaPath	0.013	0.013	0.017	0.017	0.022	**0.005**	0.007	**0.005**	0.006	0.011	
		ResNet 50	0.011	0.011	**0.005**	**0.005**	0.008	0.008	0.010	0.007	0.014	0.021	
	Kappa	UNI v1	0.027	0.022	0.011	0.021	0.013	0.021	0.013	0.018	0.013	**0.005**	UNI v1+USD (Poly)
		UNI v2	0.025	0.018	0.011	**0.007**	0.010	0.012	0.013	0.010	0.017	0.008	
		GigaPath	0.045	0.013	0.019	0.019	0.021	0.011	0.012	**0.007**	0.010	0.011	
		ResNet 50	0.031	0.029	0.017	**0.009**	0.012	0.014	0.020	0.013	0.013	0.034	
	ECE	UNI v1	0.016	0.015	**0.005**	0.034	0.009	0.014	0.011	0.013	0.019	0.008	ResNet 50+USD (ER)
		UNI v2	0.017	0.014	0.014	0.030	0.011	0.009	0.017	0.037	0.010	**0.007**	
		GigaPath	0.012	0.017	**0.008**	0.018	0.012	0.020	0.011	0.034	0.013	0.019	
		ResNet 50	0.013	0.011	0.005	0.011	0.012	**0.004**	0.015	0.009	**0.004**	0.009	

Table 16: Benchmarking standard deviation under the full metric list for the classification task.

Metrics	Methods	HEST-1K						STImage-1K4M	
		IDC	READ	PRAD	LYMPH_IDC	COAD	CCRCC	Brain	Skin
SPCC	MSE	0.009	0.007	**0.000**	0.074	0.007	0.004	0.001	0.010
	Huber	0.006	0.010	0.003	0.008	**0.001**	0.002	**0.001**	0.015
	PCCMSE	0.005	0.006	0.002	0.008	**0.001**	0.002	**0.001**	0.021
	USD (er)	0.005	0.005	0.003	0.036	**0.002**	0.006	**0.002**	0.007
GPCC	MSE	0.008	0.003	**0.002**	0.138	0.005	0.005	0.003	0.027
	Huber	0.004	0.004	0.003	0.003	**0.002**	0.008	0.004	0.066
	PCCMSE	**0.002**	0.003	0.005	**0.002**	**0.002**	0.003	0.005	0.008
	USD (er)	0.003	0.004	0.008	0.026	**0.002**	0.008	**0.002**	0.026
MSE	MSE	0.073	0.004	**0.001**	0.035	0.013	**0.001**	**0.001**	0.011
	Huber	0.065	0.002	0.002	0.005	0.009	**0.001**	**0.001**	0.035
	PCCMSE	0.025	0.003	0.002	0.007	0.002	**0.000**	0.002	0.016
	USD (er)	0.069	0.018	0.004	0.022	0.006	0.007	**0.003**	0.020

Table 17: Benchmarking standard deviation for the full metric list based on the regression task.

6.9 Comparisons between Logistic Regression and USD for Disease-State Prediction.

Here we consider a simple baseline, Logistic Regression (LR), and fit this model then make a comparison with our proposed model, to demonstrate the necessity of using the more advanced approach to address the disease-state classification task. According to Table 18, our proposed method performs better than LR in all of the included metrics across three datasets, and thus we demonstrate the necessity of developing a novel solution for this task.

6.10 Comparisons between USD and Task-Specific Method DeepPT for Gene Expression Prediction.

Here we include the comparison between our proposed method and a task-specific method DeepPT, which was benchmarked in a recent publication for gene expression prediction from histopathology images and ranked as the best method Zhang et al. (2025). DeepPT encodes a patch into embedding space with pre-trained models, and later trains an auto-encoder to make the image embeddings become more dense, and the compressed embeddings are used for predicting gene expression levels. According to Table 19, USD performs better than DeepPT evaluated by all metrics on average, and participially in the READ and the LYMPH_IDC datasets. Table 20 shows that USD is also a robust method with low variance. Therefore, USD can also surpass current state-of-the-art training pipeline.

6.11 Comparisons of Methods for Training the Prediction Head

Here we consider two modes of training the prediction head for disease-state classification based on the TCGA dataset. The first mode is full parameter training (FPT), which means we tune the feature extractor together with the prediction head. The second mode is only training the prediction head (TPH) and freezing the feature extractor, which is also the default mode with less GPU memory usage. According to Table 21, TPH performs better than FPT in all metrics, and thus we keep TPH as our final solution.

We also investigate the contribution of using patch-level (36 patches per image) information from the whole slide to train a classifier for disease-state prediction with mean pooling (MP) and multi-instance learning (ABMIL). The comparison based on the CAMELYON16 dataset with UNI v1 as base model is shown in Table 22. According to this table, using PFMs to encode slides directly is a better choice, and its required scale of training data is smaller than multi-instance learning design. The potential limitations of patch-based methods such as MP and ABMIL Ilse et al. (2018) are the bias in selecting patches to represent a slide, and the training cost of patch-level information is also more expensive. Nevertheless, our conclusion in the slide-level representation can also be transferred to patch-level representation easily, demonstrated by our

Datasets	Metrics	Base	Methods	
			LR	USD (ER)
TCGA	ACC	UNI v1	0.733	0.933
		UNI v2	0.917	1.000
		GigaPath	0.617	0.677
		ResNet 50	0.500	0.627
	AUROC	UNI v1	0.994	0.994
		UNI v2	1.000	1.000
		GigaPath	0.919	0.898
		ResNet 50	0.023	0.677
	Bacc	UNI v1	0.733	0.933
		UNI v2	0.917	1.000
		GigaPath	0.617	0.677
		ResNet 50	0.500	0.627
	Kappa	UNI v1	0.467	0.867
		UNI v2	0.833	1.000
		GigaPath	0.233	0.353
		ResNet 50	0.000	0.253
	wF1	UNI v1	0.713	0.933
		UNI v2	0.916	1.000
		GigaPath	0.551	0.627
		ResNet 50	0.333	0.613
	ECE	UNI v1	0.329	0.065
		UNI v2	0.329	0.151
		GigaPath	0.236	0.208
		ResNet 50	0.263	0.184
CAMELYON16	ACC	UNI v1	0.618	0.741
		UNI v2	0.618	0.562
		GigaPath	0.647	0.491
		ResNet 50	0.500	0.585
	AUROC	UNI v1	0.756	0.812
		UNI v2	0.751	0.753
		GigaPath	0.716	0.643
		ResNet 50	0.672	0.730
	Bacc	UNI v1	0.620	0.757
		UNI v2	0.638	0.592
		GigaPath	0.655	0.531
		ResNet 50	0.541	0.617
	Kappa	UNI v1	0.237	0.496
		UNI v2	0.264	0.173
		GigaPath	0.303	0.060
		ResNet 50	0.074	0.219
	wF1	UNI v1	0.618	0.750
		UNI v2	0.599	0.498
		GigaPath	0.646	0.350
		ResNet 50	0.376	0.524
	ECE	UNI v1	0.251	0.107
		UNI v2	0.220	0.159
		GigaPath	0.227	0.199
		ResNet 50	0.181	0.137
PANDA	ACC	UNI v1	0.458	0.495
		UNI v2	0.448	0.488
		GigaPath	0.449	0.473
		ResNet 50	0.378	0.430
	wF1	UNI v1	0.448	0.479
		UNI v2	0.438	0.488
		GigaPath	0.439	0.455
		ResNet 50	0.307	0.397
	Bacc	UNI v1	0.408	0.437
		UNI v2	0.398	0.428
		GigaPath	0.405	0.414
		ResNet 50	0.280	0.368
	Kappa	UNI v1	0.569	0.594
		UNI v2	0.551	0.603
		GigaPath	0.556	0.577
		ResNet 50	0.286	0.527
	ECE	UNI v1	0.175	0.043
		UNI v2	0.206	0.034
		GigaPath	0.142	0.031
		ResNet 50	0.045	0.022

Table 18: Evaluation results between LR and USD (ER).

Metircs	Methods	Datasets and Statistics								
		IDC	READ	PRAD	LYMPH_IDC	COAD	CCRCC	Brain	Skin	Average
SPCC	DeepPT	0.579	0.314	0.688	0.084	0.611	0.379	0.603	0.389	0.456
	USD (ER)	**0.589**	**0.381**	**0.689**	**0.129**	**0.622**	**0.386**	**0.618**	**0.409**	**0.478**
GPCC	DeepPT	0.386	0.186	0.110	0.223	0.563	0.263	0.110	0.189	0.254
	USD (ER)	**0.400**	**0.283**	**0.138**	**0.236**	**0.565**	**0.273**	**0.154**	**0.265**	**0.289**
MSE	DeepPT	2.947	0.277	0.296	0.868	0.986	**0.491**	0.282	1.668	0.977
	USD (ER)	**2.754**	**0.269**	**0.294**	**0.857**	**0.957**	0.492	**0.279**	**1.481**	**0.923**

Table 19: Comparing average scores between DeepPT and USD for the gene expression prediction task.

Metircs	Methods	Datasets and Statistics								
		IDC	READ	PRAD	LYMPH_IDC	COAD	CCRCC	Brain	Skin	Average
SPCC	DeepPT	**0.004**	**0.003**	**0.001**	**0.025**	0.003	**0.005**	0.003	0.014	**0.007**
	USD (ER)	0.005	0.005	0.003	0.036	**0.002**	0.006	**0.002**	**0.007**	0.008
GPCC	DeepPT	0.004	**0.003**	**0.006**	**0.026**	0.004	0.013	0.013	**0.015**	0.011
	USD (ER)	**0.003**	0.004	0.008	**0.026**	**0.002**	**0.008**	**0.002**	0.026	**0.010**
MSE	DeepPT	**0.027**	**0.002**	**0.001**	**0.015**	0.009	**0.001**	**0.001**	**0.016**	**0.009**
	USD (ER)	0.069	0.018	0.004	0.022	**0.006**	0.007	0.003	0.020	0.019

Table 20: Comparing standard deviation between DeepPT and USD for the gene expression prediction task.

Metrics	FPT	TPH
Acc	0.487 (0.014)	0.912 (0.020)
AUROC	0.600 (0.236)	0.984 (0.010)
Bacc	0.487 (0.014)	0.900 (0.038)
Kappa	-0.028 (0.028)	0.827 (0.043)
wF1	0.327 (0.006)	0.913 (0.022)

Table 21: Performances of two modes for training the prediction head. The format of value in the table is: average (standard deviation).

regression-based experiments. Moreover, we consider removing samples which are wrongly classified by the linear classifier and re-train the prediction head (RD), whose result is also summarized in this table. We find that removing difficult samples cannot improve model performance, and thus our default setting is the most optimal setting. With the same dataset, we also consider a different approach to compute $\mathcal{MRMD}$, that is, for a sample with class c, we compute the base Gaussian model G_b based on the samples not belonging to this class. This approach is represented as $\mathcal{MRMD}$ (class removal) and the default method is represented as $\mathcal{MRMD}$ (base). According to Table x, $\mathcal{MRMD}$ (base) has better performances, and thus using different types of samples to compute $\mathcal{MRMD}$ also does not improve the performance of USD.

Datasets	**Metrics**	**Methods**			
		MP	RD	ABMIL	Default
CAMELYON16	ACC	0.524 (0.035)	0.562 (0.048)	0.509 (0.017)	0.756 (0.022)
	AUROC	0.643 (0.060)	0.641 (0.048)	0.538 (0.018)	0.834 (0.020
	Bacc	0.542 (0.026)	0.580 (0.055)	0.071 (0.033)	0.771 (0.019)
	Kappa	0.082 (0.052)	0.152 (0.103)	0.448 (0.037)	0.525 (0.040)
	wF1	0.496 (0.060)	0.537 (0.052)	0.618 (0.059)	0.750 (0.027)
	ECE	0.212 (0.033)	0.188 (0.046)	0.267 (0.039)	0.107 (0.019)

Table 22: Performances of four different strategies for training the prediction head. The format of value in the table is: average (standard deviation).

Datasets	**Metrics**	**Methods**	
		$\mathcal{MRMD}$ (base)	$\mathcal{MRMD}$ (class-removal)
CAMELYON16	ACC	0.756 (0.022)	0.750 (0.021)
	AUROC	0.834 (0.020	0.831 (0.009)
	Bacc	0.771 (0.019)	0.767 (0.018)
	Kappa	0.525 (0.040)	0.514 (0.038)
	wF1	0.750 (0.027)	0.743 (0.025)
	ECE	0.107 (0.019)	0.109 (0.154)

Table 23: Performances of two different strategies for computing sample difficulty. The format of value in the table is: average (standard deviation).

6.12 Effect of choosing the cluster number

Since the ASW score is widely used in evaluating the clustering performance in spatial transcriptomic data analysis, we believe that the biological signals will not be oversimplified by selecting the optimal bin number. We present additional experimental results by using different numbers of bins for KMeans clustering after processing the data with Harmony, and the image features are extracted with UNI v2. Table 24 shows that selecting the best k based on tuning ASW score achieves the highest SPCC score in over 75% datasets from both the HEST and STImage1k4M databases, and its GPCC and MSE are also in the top2 list for most of the datasets. Moreover, using the best k can obviously reduce the randomness and improve training robustness evaluated with all three metrics, especially in the IDC and LYMPH_IDC datasets, since the results based on k=7 and 11 for IDC and k=5 and 7 for Brain show high variance in the evaluation with MSE or SPCC across five random seeds. Therefore, tuning the cluster number k with ASW score is an effective approach to select the size used for model training, supported by its superiority in average performance and robustness.

Dataset (best k)	Metric	k=3	k=5	k=7	k=9	k=11
IDC (best k=3)	SPCC	0.591 (0.004)	0.590 (0.003)	0.591 (0.007)	0.591 (0.008)	0.589 (0.008)
	GPCC	0.400 (0.003)	0.401 (0.004)	0.396 (0.004)	0.403 (0.002)	0.398 (0.008)
	MSE	2.69 (0.005)	2.70 (0.083)	2.80 (0.173)	2.75 (0.067)	2.76 (0.150)
READ (best k=3)	SPCC	0.381 (0.005)	0.383 (0.005)	0.379 (0.006)	0.379 (0.004)	0.383 (0.010)
	GPCC	0.283 (0.004)	0.285 (0.001)	0.282 (0.002)	0.286 (0.005)	0.285 (0.004)
	MSE	0.269 (0.018)	0.270 (0.012)	0.265 (0.009)	0.267 (0.011)	0.270 (0.004)
PRAD (best k=3)	SPCC	0.690 (0.003)	0.687 (0.003)	0.686 (0.002)	0.686 (0.004)	0.689 (0.003)
	GPCC	0.138 (0.008)	0.134 (0.006)	0.132 (0.004)	0.136 (0.009)	0.138 (0.003)
	MSE	0.294 (0.004)	0.293 (0.004)	0.295 (0.002)	0.294 (0.003)	0.291 (0.002)
LYMPH_IDC (k=7)	SPCC	0.119 (0.051)	0.120 (0.049)	0.129 (0.036)	0.136 (0.046)	0.101 (0.044)
	GPCC	0.241 (0.020)	0.239 (0.018)	0.236 (0.026)	0.250 (0.006)	0.205 (0.052)
	MSE	0.864 (0.025)	0.862 (0.019)	0.857 (0.022)	0.872 (0.020)	0.852 (0.023)
COAD (best k=3)	SPCC	0.622 (0.002)	0.625 (0.002)	0.625 (0.003)	0.624 (0.005)	0.623 (0.004)
	GPCC	0.565 (0.002)	0.567 (0.003)	0.568 (0.002)	0.567 (0.002)	0.565 (0.004)
	MSE	0.957 (0.006)	0.958 (0.003)	0.959 (0.005)	0.953 (0.009)	0.959 (0.010)
CCRC (best k=3)	SPCC	0.386 (0.006)	0.383 (0.003)	0.383 (0.007)	0.386 (0.011)	0.382 (0.006)
	GPCC	0.273 (0.008)	0.274 (0.005)	0.272 (0.007)	0.273 (0.008)	0.270 (0.007)
	MSE	0.492 (0.007)	0.492 (0.004)	0.494 (0.001)	0.493 (0.005)	0.495 (0.004)
Brain (best k=3)	SPCC	0.618 (0.002)	0.613 (0.008)	0.610 (0.008)	0.610 (0.007)	0.612 (0.007)
	GPCC	0.154 (0.002)	0.157 (0.007)	0.155 (0.008)	0.157 (0.010)	0.161 (0.010)
	MSE	0.279 (0.003)	0.279 (0.004)	0.280 (0.005)	0.281 (0.005)	0.276 (0.003)
Skin (best k=3)	SPCC	0.409 (0.007)	0.395 (0.021)	0.390 (0.023)	0.396 (0.013)	0.409 (0.009)
	GPCC	0.265 (0.020)	0.255 (0.019)	0.262 (0.019)	0.255 (0.020)	0.258 (0.025)
	MSE	1.481 (0.020)	1.580 (0.014)	1.572 (0.013)	1.589 (0.025)	1.581 (0.010)

Table 24: Effect of cluster number k with format score (standard deviation) for the regression task.

6.13 Comparisons between USD (ER) and USD (Poly) for the Gene Expression Prediction.

The results for comparing two modes of USD are shown in Figure 8. According to this figure, these two modes do not show obvious differences across all selected metrics.

6.14 Comparisons between Different Base Models for Gene Expression Prediction

According to Tables 25 and 26, UNI v2-based combination always outperforms other combinations evaluated by GPCC, and it also has low variance. Therefore, UNI v2 is selected as the base model for evaluating the performances of gene expression prediction based on different training strategies.

6.15 Broader Impact and Limitations

One possible limitation of USD could be the task-specific requirements of pathology foundation models, as the sample difficulty is affected by the source representations, and thus different foundation models might lead to differences in estimating sample difficulty. One potential solution is to define a metric to select models before estimating sample difficulty. The other limitation could be training efficiency for large-scale datasets, which could potentially be addressed by using advanced GPU cores.

6.16 Ablation studies

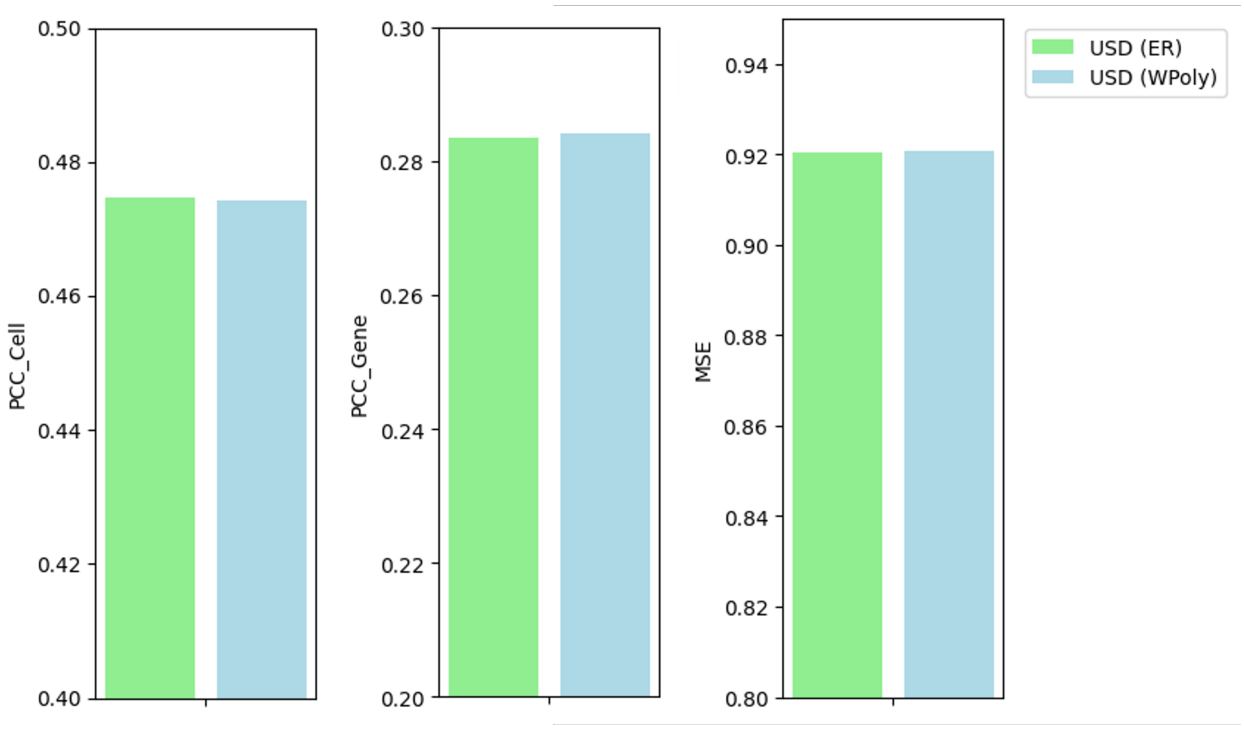

Figure 8: Benchmarking scores averaged by all tested datasets between USD (ER) and USD (Poly).

Metrics	Methods	Base Models			
		UNI v1	UNI v2	GigaPath	ResNet 50
SPCC	MSE Loss	0.572	0.581	**0.588**	0.550
	Huber Loss	0.562	**0.589**	0.585	0.527
	PCCMSE Loss	0.575	0.588	**0.599**	0.554
GPCC	MSE Loss	0.348	**0.389**	0.330	0.267
	Huber Loss	0.334	**0.390**	0.321	0.220
	PCCMSE Loss	0.355	**0.400**	0.351	0.281
MSE	MSE Loss	3.424	2.825	2.945	**2.598**
	Huber Loss	3.512	**2.812**	2.951	2.919
	PCCMSE Loss	3.414	2.748	2.855	**2.561**

Table 25: Benchmarking average scores for the full metric list based on different base models for the regression task.

Metrics	Methods	Base Models			
		UNI v1	UNI v2	GigaPath	ResNet 50
SPCC	MSE Loss	0.013	0.009	**0.004**	0.006
	Huber Loss	0.010	**0.006**	**0.006**	0.007
	PCCMSE Loss	0.006	0.005	0.005	**0.002**
GPCC	MSE Loss	**0.002**	0.008	0.017	0.019
	Huber Loss	0.008	**0.004**	0.006	0.016
	PCCMSE Loss	0.003	**0.002**	0.007	0.003
MSE	MSE Loss	**0.034**	0.073	0.059	0.043
	Huber Loss	**0.026**	0.065	0.075	0.079
	PCCMSE Loss	0.030	**0.025**	0.032	0.031

Table 26: Benchmarking standard deviation for the full metric list based on different base models for the regression task.

Metrics	Methods	Datasets								
		IDC	READ	PRAD	LYMPH_IDC	COAD	CCRCC	Brain	Skin	Average
SPCC (↑)	$L_{\text{base}} + L_{\text{OE}}$	**0.591**	0.359	0.689	0.127	**0.624**	0.381	0.617	0.406	0.474
	$L_{\text{base}} + L_f$ (CE)	0.586	0.376	0.689	0.072	0.620	0.381	0.616	0.398	0.467
	$L_{\text{base}} + L_{\text{OE}} + L_f$ (CE)	0.589	0.373	**0.689**	0.076	0.616	0.376	0.614	0.408	0.468
	$L_{\text{base}} + L_{\text{OE}} + L_f$	0.589	**0.381**	0.689	**0.129**	0.622	**0.386**	**0.618**	**0.409**	**0.478**
GPCC (↑)	$L_{\text{base}} + L_{\text{OE}}$	0.400	0.271	0.136	0.234	**0.567**	0.266	0.151	0.264	0.286
	$L_{\text{base}} + L_f$ (CE)	0.395	0.280	0.134	0.228	0.565	**0.275**	0.138	**0.272**	0.286
	$L_{\text{base}} + L_{\text{OE}} + L_f$ (CE)	0.398	0.267	0.131	0.216	0.563	0.267	0.149	0.262	0.282
	$L_{\text{base}} + L_{\text{OE}} + L_f$	**0.400**	**0.283**	**0.138**	**0.236**	0.565	0.273	**0.154**	0.265	**0.289**
MSE (↓)	$L_{\text{base}} + L_{\text{OE}}$	2.718	**0.242**	0.294	0.860	**0.956**	**0.488**	0.293	1.516	0.921
	$L_{\text{base}} + L_f$ (CE)	2.790	0.255	**0.293**	0.832	0.968	0.495	0.287	1.562	0.935
	$L_{\text{base}} + L_{\text{OE}} + L_f$ (CE)	**2.694**	0.291	0.302	**0.737**	0.972	0.492	0.312	1.487	**0.911**
	$L_{\text{base}} + L_{\text{OE}} + L_f$	2.754	0.269	0.294	0.857	0.957	0.492	**0.279**	**1.481**	0.923

Table 27: Benchmarking results for different PCCMSE variants in the regression task as ablation studies. We report the average scores (Average) across datasets. The best score for each dataset is boldfaced. For SPCC and GPCC, higher values indicate better performance; for MSE, lower values indicate better performance.